Microfluidic Devices for Genomic Analysis

Lotien Richard Huang

A dissertation presented to the faculty

of Princeton University in candidacy

for the degree of Doctor of philosophy

Recommended for acceptance

by the Department of

Electrical Engineering

October 2003

Supported by grants from DARPA (MDA972-00-1-0031), NIH (HG01506), and the State of New Jersey (NJCST 99-100-082-2042-007).

Dedicated to my parents and friends

ABSTRACT

Separation by size is a fundamental analytical and preparative technique in biology, medicine, chemistry, and industry. Fractionation of biological molecules, such as nucleic acids and proteins, plays a central role in genomic analysis. In the post-genomic era, this task becomes ever more important because solving the puzzle of interactions between proteins is far more complicated than deciphering genomes, due to the lack of proteins' equivalent of amplification, fractionation and sequencing techniques.

Micro- and nano-fabricated structures offer many possibilities to improve our ability to manipulate and probe biological molecules. In this thesis, we first discuss how microfabricated Brownian ratchets are used for separation of molecules, including nucleic acids. More specifically, our contribution to this field includes clarifying the role of particle size in the ratchet array operations. Further, we improved by an order of magnitude the separation speed and resolution of such arrays, whose usefulness had been limited by the slow separation speed and poor resolution. The improvement is a result of flow tilting—adjusting the flow direction with respect to the array orientation.

Related to flow tilting, we present a new method for particle separation according to size, with ultrahigh speed and resolution. The method uses an ordered array of obstacles and a driving flow, which is aligned at an angle with respect to the array. The flow undergoes series of uneven bifurcations at the obstacles. Particles in such a flow moves in one of the two distinct modes of migration, depending on their sizes. Submicrometer-

sized particles were separated with 1% resolution in 40 s. The physical mechanism of the separation process is presented.

Although the tango array separates rigid particles with astonishingly high resolutions, its resolving power for DNA molecules is considerably lower, because DNA fragments coil in arbitrary shapes, and become stretched unequally when interacted with the tango array. A different microfluidic device for DNA separation, the DNA prism, is introduced. The DNA prism separates ~100 kb DNA 1000 times faster than conventional methods, and provides solutions to sample loading and field uniformity problems. A physical model for explaining the complicated separation characteristics of DNA prisms is developed. The model assumes that DNA molecules in such devices act as damped springs, which change their lengths in response to the applied electric pulses, instead of a rigid chain, as assumed in prior works. As a result of this model, conditions for improved separation characteristics are found.

ACNOWLEDGEMENTS

Acknowledging the people who helped me through the five years of graduate study at Princeton is difficult, because without any one of them, I might not have enjoyed such a wonderful and worthwhile time of my life. I would like to thank my academic advisor Prof. **James C. Sturm** for his help, guidance and support, without which this endeavor would have been impossible. Equally important are my collaborating advisors, Prof. **Robert H. Austin** and Prof. **Edward C. Cox**, with whose generous help and guidance, this endeavor became more valuable and intellectually challenging. I would also like to thank Prof. **Steven Y. Chou** for reading this thesis.

Words cannot describe my appreciation for the encouragement and support from my parents. It has been a long journey with its share of excitements and frustrations—studying in a new environment and culture is not always easy—and my parents always give me the strength to move on.

I would like to thank **Ming Yang**, **Mike Lu**, and all members of the Sturm group for their help and discussion about our laboratory, research and graduate study in general. It made the whole graduate student experience wonderful.

A special thank you goes to all the members in Prof. Austin's group, especially to **Jonas Tegenfeldt**, **Christelle Prinz**, **Sungsu Park**, **Pascal Silberzan** and **Olgica Bakajin**, for their help, discussion, inspiration and suggestions.

I would like to thank all members in Prof. Cox's group, especially **Jessica J. Kraeft,** for their help and discussion. It made the whole graduate student experience wonderful.

The faculty and staff of the EMD group here at Princeton are instrumental in creating the good atmosphere for research. I would like to thank **Mike Valenti**, **Joe Palmer**, **Duane Marcy** and **Helena Gleskova** for their help with cleanroom operations, and **Nan Yao** for scanning electron microscopy.

Finally, no acknowledgment would be complete without thanking all my friends, especially **Bing Wang**, **Allan Chang** and **Maggie Chiang**, who generously offered help when I need it, and who made my stay at Princeton a special and unforgettable experience.

TABLE OF CONTENTS

Chapter 1

Introduction

1.1 Background and Motivation

Separation by size is a fundamental analytical and preparative technique in biology, medicine, chemistry, and industry. Fractionation of biological molecules, such as nucleic acids and proteins, plays a central role in genomic analysis. In the post-genomic era, this task becomes ever more important because solving the puzzle of interactions between proteins is far more complicated than deciphering genomes, due to the lack of proteins' equivalent of amplification, fractionation and sequencing techniques.

Conventional methods for molecular separation include gel electrophoresis, field-flow fractionation, sedimentation, and size exclusion chromatography [1]. Gel electrophoresis utilizes an electric field to drive charged molecules to be separated through a gel medium, which serves as a sieving matrix. The molecules are initially loaded at one end of a gel matrix, and are separated into components zones as they migrate through the gel.

Field-flow fractionation is carried out in a thin ribbon-like channel, in which the flow profile is parabolic [2]. Particles are loaded as a sample zone, and then flown through the channel. Separation occurs because particles of different properties flow in different positions of the flow, due to the influence of a field, resulting in different migration speeds. The field is applied perpendicular to the flow.

Sedimentation utilizes gravitational or centrifugal acceleration to force particles through a fluid. Particles migrate through the fluid at different speeds, depending on their sizes and densities, and thus are separated.

Size exclusion chromatography (SEC) utilizes a tube packed with porous beads, through which sample molecules are washed. Molecules smaller than the pores can enter the beads, which lengthens their migration path, whereas those larger than the pores can only flow between the beads. In this way smaller molecules are on average retained longer and thus become separated from larger molecules [3].

Micro- and nano-fabricated structures offer many possibilities to improve our ability to manipulate and probe biological molecules such as DNA and proteins [4–10]. A first advantage of such approaches over conventional methods is that they can greatly increase the speed and integration levels and reduce the cost of conventional methods, enabling more widespread applications such as clinical point-of-care analysis. Second, the ability to manipulate and analyze single molecules enables one to study single molecules and the contents of single cells, enabling one to probe the heterogeneity that inherently exists

within even genetically identical populations. Third, the small physical size can be used to enable methods not possible with conventional analysis, such as direct spatial imaging within genomes.

In microfluidic approaches for manipulating biological molecules, the conventional test tubes and pipettes are replaced by miniaturized plumbing channels (with 0.1- to 100-μm dimensions) etched into the surface of a wafer using methods borrowed from the integrated circuit industry, such as photolithography and reactive ion etching [11, 12]. In the simplest approaches, the tops of channels are sealed by bonding a flat cover slip to the top of the etched structure. Not only does this approach reduce the analysis volumes, but the integration of electrodes also enables one to use electric fields to drive ion and molecular flows (termed "electrophoresis") in addition to the possible application of pressure.

1.2 Thesis Outline

In the next chapter, we will discuss how microfabricated Brownian ratchets are used for separation of molecules, including nucleic acids. A Brownian ratchet is a structure which permits Brownian motion in only one direction [13, 14]. It is a device that harnesses Brownian motion, which is usually considered detrimental, for molecular separation. However, because Brownian ratchets intrinsically depend on molecular diffusion, the separation process using such ratchets is time-consuming, with running times typically of 2 hours [15–19].

In Chapter 3, we will discuss a general and effective method for optimizing the speed and resolution of Brownian ratchets. The key factor to be adjusted in the optimization process is the flow direction with respect to the ratchet structure. We increased the separation speed and resolution of the ratchet design in Chapter 2 by an order of magnitude, using this method [20].

During the research on optimizing Brownian ratchet arrays, we observed a flow effect which can be used for particles separation, and which does not rely on diffusion. This effect is interesting in light of its application to particles separation, because the separation process could occur rapidly. In fact, as we will see in Chapter 4, this flow effect allows for separation of submicrometer-sized particles with 1% resolution in 40 s. The obstacle array that utilizes the flow effect is referred to as the microfluidic tango array.

Although the tango array separates rigid particles with astonishingly high resolutions, its resolving power for DNA molecules is considerably lower, because DNA fragments coil in arbitrary shapes, and become stretched unequally when interacted with the tango array. A different microfluidic device for DNA separation, the DNA prism, will be the topic of Chapter 5 to Chapter 7 [21].

Chapter 5 introduces a method for generating tunable uniform electric field across the sieving matrix of the DNA prism. Generating uniform field had been a main

technological hurdle to construct such a device. The current injection method utilizes microfluidic channels as electric current sources for imposing proper boundary conditions for uniform fields [22].

Chapter 6 discusses fractionation of genomic-sized DNA molecules, using the DNA prism. More specifically, bacterial artificial chromosomes are sorted according to size with great speeds [21]. Separation of these chromosomes had always been time-consuming, using conventional methods [23–27].

Chapter 7 presents a physical model for explaining the complicated separation characteristics of DNA prisms [28]. The model assumes that DNA molecules in such devices act as damped springs, which change their lengths in response to the applied electric pulses, instead of a rigid chain, as assumed in prior works. As a result of this model, conditions for improved separation characteristics are found.

Finally we summarize our contributions and make suggestions for future work in this field in Chapter 8.

References

1. J. C. Giddings, *Unified Separation Science* (Wiley, New York, 1991).
2. J. C. Giddings, *Science* **260**, 1456 (1993).
3. J. C. Giddings, *Nature* **184**, 357 (1959).
4. W. D. Volkmuth and R. H. Austin, *"DNA Electrophoresis in Microlithographic Arrays," Nature* **358**, 600 (1992).
5. M. Schena, D. Shalon, R. W. Davis, and P. O. Brown, *"Quantitative Monitoring of Gene Expression Patterns with a Complementary DNA Microarray," Science* **270**, 467 (1995).
6. M. A. Burns, B. N. Johnson, S. N. Brahmasandra, K. Handique, J. R. Webster, M. Krishnan, T. S. Sammarco, P. M. Man, D. Jones, D. Heldsinger, C. H. Mastrangelo, and D. T. Burke, *"An Integrated Nanoliter DNA Analysis Device," Science* **282**, 484 (1998).
7. M. U. Kopp, A. J. de Mello, and A. Manz, *"Chemical Amplification: Continuous-Flow PCR on a Chip," Science* **280**, 1046 (1998).
8. A. Hatch, A. E. Kamholz, K. R. Hawkins, M. S. Munson, E. A. Schilling, B. H. Weigl, P. Yager, *"A rapid diffusion immunoassay in a T-sensor," Nature Biotechnology* 19, 461 (2001).
9. T. Thorsen, S. J. Maerkl, and S. R. Quake, *"Microfluidic Large-Scale Integration," Science* **298**, 580 (2002).
10. D. L. Huber, R. P. Manginell, M. A. Samara, B. Kim, and B. C. Bunker, *"Programmed Adsorption and Release of Proteins in a Microfluidic Device," Science* **301**, 352 (2003).
11. E. W. Becker *et. al*., Microelectronic Engineering 4 (1986), pages 35 to 56.
12. H. Becker *et. al*., J. Micromech. Microeng. 8 (1998), pages 24 to 28.
13. Feynman, R. P.; Leighton, R. B.; Sands, M. *The Feynman Lectures On Physics* Ch. 46 **Vol. 1** (Addison-Wesley, Reading, Massachusetts, 1966)
14. Astumian, R. D. *Science* **1997**, *276*, 917–922.
15. Duke, T. A. J.; Austin, R. H. *Phys. Rev. Lett.* **1998**, *80*, 1552–1555.
16. Ertas, D. *Phys. Rev. Lett.* **1998**, *80*, 1548–1551.
17. van Oudenaarden, A.; Boxer, S. G. *Science* **1999**, *285*, 1046–1048.
18. C. F. Chou, O. Bakajin, S. Turner, T. Duke, S. S. Chan, E. C. Cox, H. G. Craighead, and R. H. Austin, *"Sorting by Diffusion: An Asymmetric Obstacle Course for Continuous Molecular Separation", Proc. Natl. Acad. Sci.* USA **96** (24): 13762 (1999)
19. Huang, L. R.; Silberzan, P; Tegenfeldt, J. O.; Cox, E. C.; Sturm, J. C.; Austin, R. H.; Craighead H. *Phys. Rev. Lett.* **2002**, *89*, 178301–178304.
20. L. R. Huang, E. C. Cox, R. H. Austin, J. C. Sturm, *"A Tilted Bownian Ratchet for DNA Analysis," Analytical Chemistry* (Accepted as of Sep. 2003).
21. L. R. Huang, J. O. Tegenfeldt, J. J. Kraeft, J. C. Sturm, R. H. Austin, E. C. Cox, *"A DNA Prism for High-Speed Continuous Fractionation of Large DNA Molecule," Nature Biotechnology* **20(10)**, 1048 (2002).

22. Huang, L. R. *et. al., "Generation of large-area tunable uniform electric fields in microfluidic arrays for rapid DNA separation." International Electron Devices Meeting Technical Digest*, 363-366 (2001).
23. Carle, G. F., Frank M. & Olson, M. V. *"Electrophoretic separations of large DNA molecules by periodic inversion of the electric field." Science* **232**, 65-68 (1986).
24. Schwartz, D. C. & Cantor, C. R. *"Separation of yeast chromosome-sized DNAs by pulsed field gradient gel electrophoresis." Cell* **37**, 67-75 (1984).
25. Chu, G., Vollrath, D. & Davis, R. W. *"Separation of large DNA molecules by contour-clamped homogeneous electric fields."* *Science* **234**, 1582-1585 (1986).
26. Cox, E. C., Vocke, C. D. & Walter S. *"Electrophoretic karyotype for Dictyostelium discoideum."* *Proc. Natl. Acad. Sci. U.S.A.* **87** (21), 8247-8251 (1990).
27. Sambrook, J., Fritsch, E. F. & Maniatis, T. *Molecular Cloning: A Laboratory Manual, second edition*. (Cold Spring Harbor Laboratory Press, Cold Spring Harbor, NY)
28. L. R. Huang, *et. al, "A DNA Prism: Physical Principles for Optimizing a Microfabricated DNA Separation Device," International Electron Devices Meeting Technical Digest*, 211 (2002).

Chapter 2

Brownian Ratchet Arrays for Molecular Fractionation

2.1 Introduction

It has been proposed that an array of spatially asymmetric obstacles could operate as Brownian ratchets, structures that permit Brownian motion in only one direction [1–7]. When particles flow through such an array driven by an electric field (Fig. 2.1A), particles diffusing to the left (path 1; Fig. 2.1A) are blocked and deflected back to gap B, whereas those diffusing to the right (path 2) are deflected to gap B+. The probability of deflection depends on diffusion coefficient of the particle. Small molecules thus have a higher probability of being ratcheted than larger ones, and they in average migrate at a greater angle with respect to the vertical axis. A major advantage of the Brownian ratchet array is that in principle, it can separate molecules according only to their diffusion coefficients, without having to make assumptions about the shapes or properties of the and molecules being separated. Therefore, globular and linear molecules can be sorted in the same run.

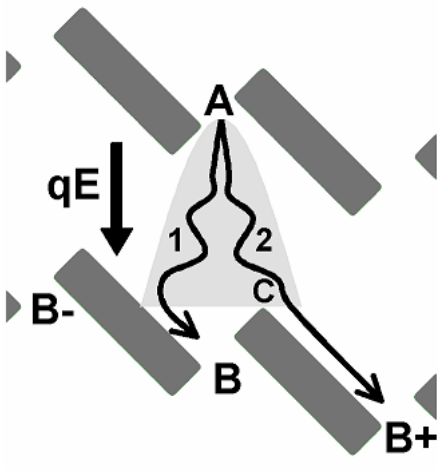

Fig. 2.1. Basic principle of the Brownian ratchet array.

Constructing such an array had been difficult because the ratcheting effect is small. It is difficult to distinguish the ratcheting effect from the flow effect, and thus the flow has to be carefully controlled. Further, samples have to be injected in a narrow stream, for the small ratcheting effect to be detected. One of the major advances presented in this dissertation is the method for controlling the flow and sample injection on the microscopic scale, which lead to the experimental realization of the proposed Brownian ratchet for DNA separation.

It was believed that Brownian ratchet arrays would work more efficiently with small molecules rather than larger ones, because small molecules diffuse more rapidly. However, my work showed that whereas DNA in the 100 kb range were separated efficiently using the ratchet, molecules in the 1 kb range did not separate at all. A theory was developed to clarify the critical role of molecular size in Brownian ratchet arrays [8].

2.2 Flow Direction and Equipotential Matching

To isolate deflection due to diffusion, it is required that all field lines through an upper gap ('A' in Fig. 2.2A) map through a lower gap ('B'), which is aligned to the upper gap. If the field lines are misaligned so that some field lines through gap A leak to gap C or D (Fig. 2.2B), we will not be able to distinguish whether a particle migrating from gap A to C is by diffusion or by following the field. This requirement has to hold over the entire array area. This occurs only for a single choice of the angle of the equipotential lines. The proper equipotential contours (Fig. 2.2A) in our array were determined by numerically solving Poisson equation using this field requirement as the boundary condition, and assuming that the obstacles are insulators. Note that although the average current flow is in the vertical direction (from A to B as shown in Fig. 2.2A), and the equipotential lines are always perpendicular to the local electric field by definition, they are not perpendicular to the average current direction and are not horizontal. If horizontal equipotential are imposed as the boundary conditions (Fig. 2.2B), a significant proportion of molecules will drift to the right, even in the absence of diffusion.

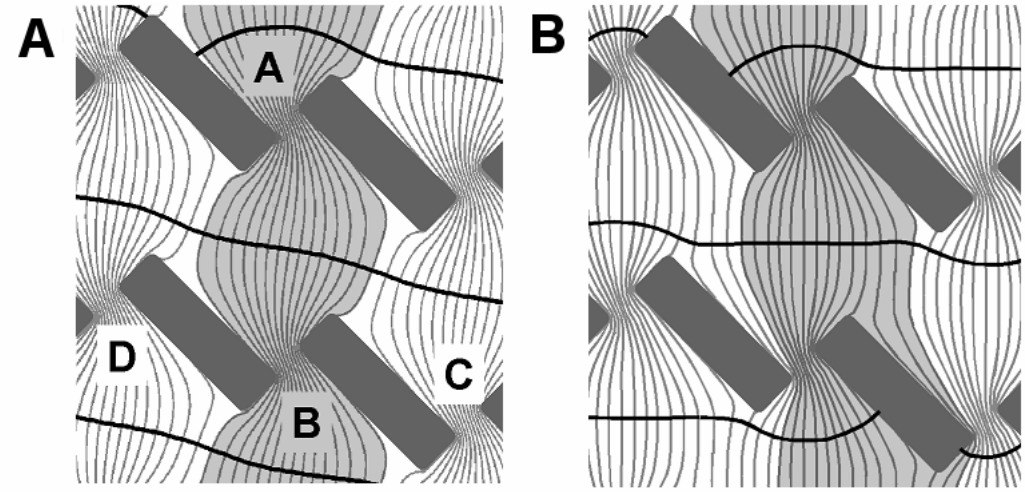

Fig. 2.2. (A) Electric field and equipotential lines with boundary conditions that all field lines flow into gap A continue through gap B. Note that the equipotential lines are not horizontal. (B) Field and equipotential lines with boundary condition of horizontal equipotentials. Note some field lines are diverted to adjacent gaps.

To generate the desired aligned current distribution of Fig. 2.2A, the array edges to which equipotentials are applied should be along the calculated equipotential direction. Therefore the array should be designed to have slanted top and bottom edges properly aligned with equipotential contours.

2.3 Sample Injection

The Brownian ratchet array device integrated with sample injection structures is schematically shown in Fig. 2.3. The array edges are designed to match the equipotential contours for vertical fields. The obstacle array does not connect directly to the aqueous buffer reservoirs, where electrodes immerse, but rather through many microfluidic channels of identical electrical resistances. Each microfluidic channel provides equal

amount of electric current, forming a uniform "curtain" of ion flow [9]. Samples are fed at a tiny spot via a single channel, which connects the array to the sample reservoir.

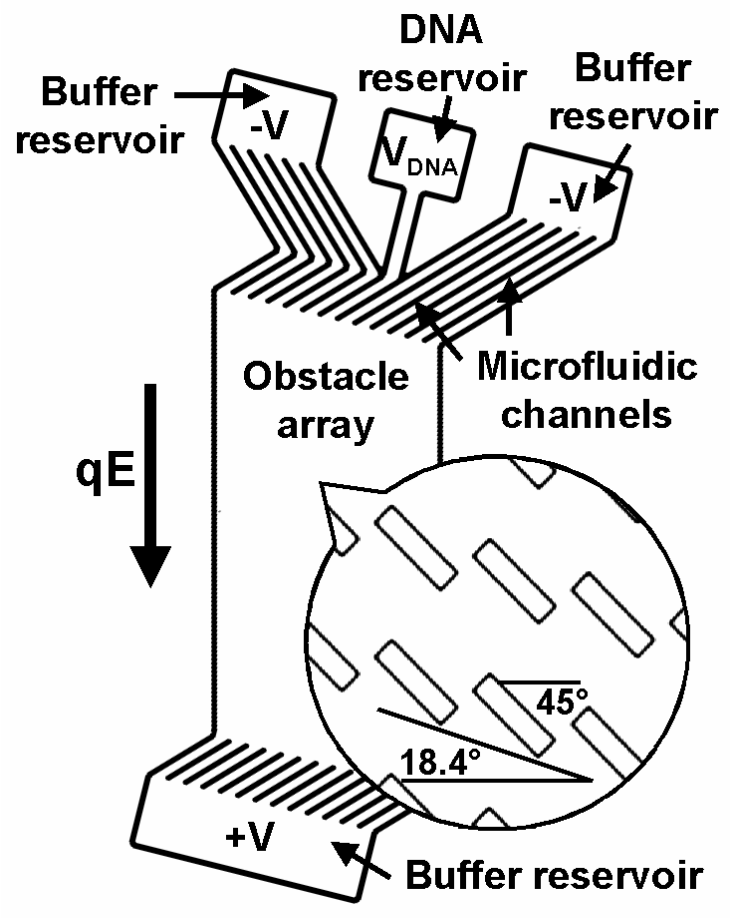

Fig. 2.3. Schematic diagram of the device. The obstacles are ~1.4 μm wide, ~5.6 μm long, and ~5 μm tall. The array is 12 mm high and 6 mm wide.

2.4 Device Fabrication

The fabrication process starts with photolithography [10–12]. A thin layer (0.9 μm) of photoresist (AZ-5209 from Clariant Corporation) was spun on a polished fused-silica

wafer and patterned with UV light. The exposed part of the photoresist was dissolved away in the developer, leaving the patterned polymer as a protective layer against the following etching step. Reactive ion etching (RIE), with a plasma discharge with CF_4 and H_2, was used to etch the exposed fused-silica surface anisotropically 2 to 6 μm deep. The wafer was then diced and the access holes contacting the reservoirs were sand-blasted through the wafer. Finally, the fused-silica die was cleaned and hermetically bonded to a piece of RTV-silicone-coated glass cover slip to form enclosed fluidic channels (RTV-615 from General Electric).

2.5 Separation of Large DNA

A mixture of coliphage λ DNA (48.5 kb, ~5 μg/ml) and coliphage T2 DNA (164 kb, ~2 μg/ml) in Tris-Borate-EDTA buffer (0.5x) was injected into the array at various speeds using electric fields. The buffer contained 0.1% POP-6, a performance optimized linear polyacrylamide (Perkin-Elmer Biosystems) to suppress electro-osmotic flow. At relative high fields (>5 V/cm), molecules move quickly (>10 μm/s), and diffusion was negligible. Molecules formed a straight band and no lateral separation occurred (Fig. 2.4A). The fact that the band did not curve even at the boundary of the array shows that the equipotential boundary conditions were properly imposed, and the current direction was well-aligned to the obstacle array.

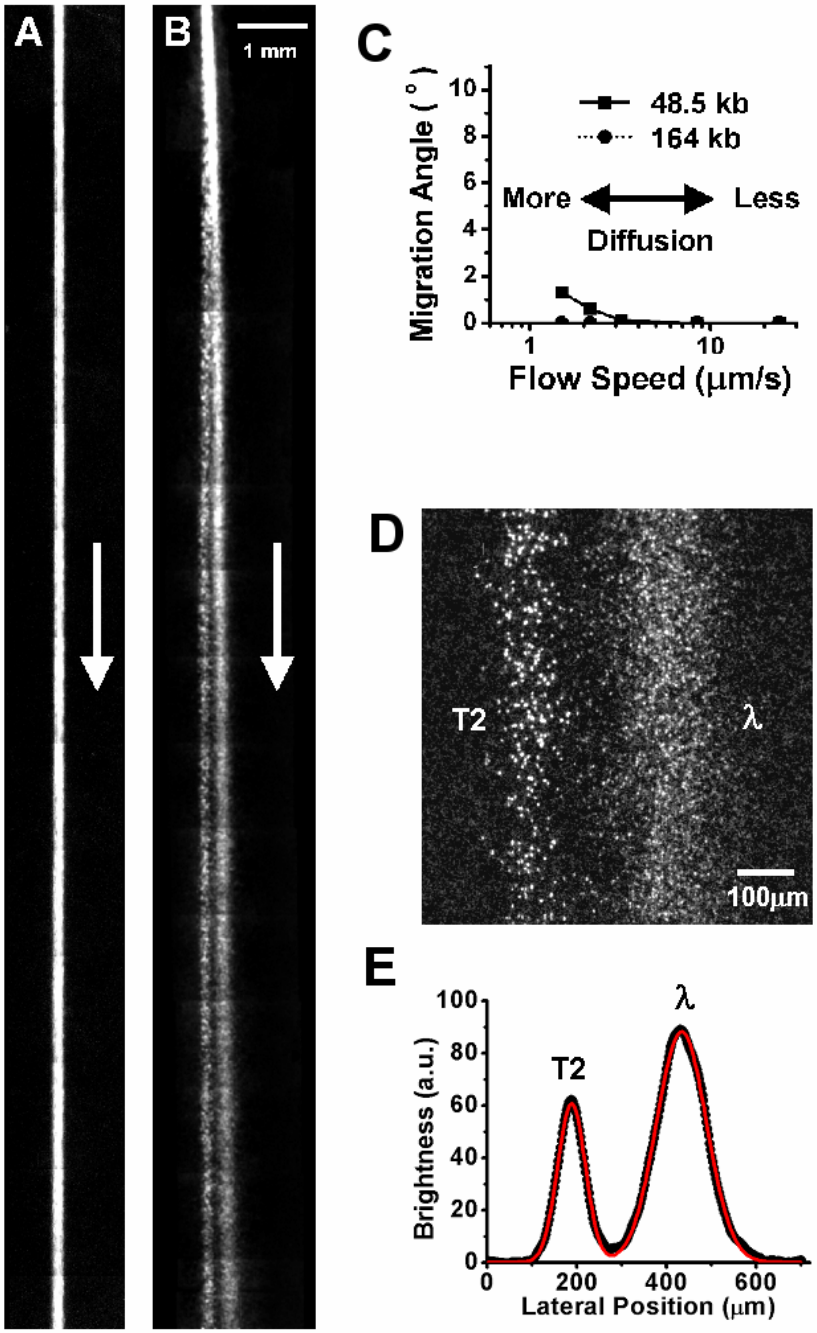

Fig. 2.4 (A) Fluorescence micrograph of coliphage λ and T2 DNA stained with the fluorescent dye TOTO-1 forming a band of ~90 μm wide and 12 mm long at ~24 μm/s. (B) Fluorescence micrograph of the two species separated into two bands at 1.5 μm/s. (C) Separation angle between λ and T2 bands as a function of flow speeds. Note the log scale of horizontal axis. (D) Zoom in of (B) at ~11 mm from the injection point. (E) Fluorescence profile of (D). Experimentat data (thick black line) fitted with two Gaussian peaks.

Lateral separation of the two species was observed at flow speeds lower than ~3 μm/s (Fig. 2.4B, C). At this flow speed, the Peclet number *Pe*, defined as (*characteristic dimension*)*(*velocity*)/(*diffusion coefficient*), is about 6 for coliphage λ DNA, and thus molecular diffusion is significant. λ molecules were deflected from the vertical more than T2 DNA. The separation became larger (~1.3^o) as the flow speed was lowered to ~1.5 μm/s (Fig. 2.4 B). The two species could be separated into two cleanly resolved bands 11 mm from the injection point, and the density profile of these bands was well fitted by two Gaussian peaks (Fig. 2.4D, E). The resolution between the two peaks, defined as ΔX / ($2\sigma_1 + 2\sigma_2$) where ΔX is the separation and σ_1 and σ_2 are the standard deviations of the peaks, was ~1.4.

2.6 Role of Molecular Size in Ratchet Fractionation

To examine the scaling of the deflection to very small molecular sizes, a mixture of 411 b (PCR product, ~1 μg/ml) and λ DNA (~20 ng/ml) was injected into an array of $\theta_{tilt} = 0^o$, at flow speeds ranging from 12 μm/s to 240 μm/s. At these flow conditions, λ DNA molecules do not deviate from the field direction (Fig. 2.4), and thus are used to label the flow direction. The Peclet number *Pe* for the 411 b molecules in these flow speeds ranges from ~1 to 20, and thus deflection should be observed. However, contrary to our expectations based on Fig. 2.1 [3, 4], absolutely no lateral deflection was observed.

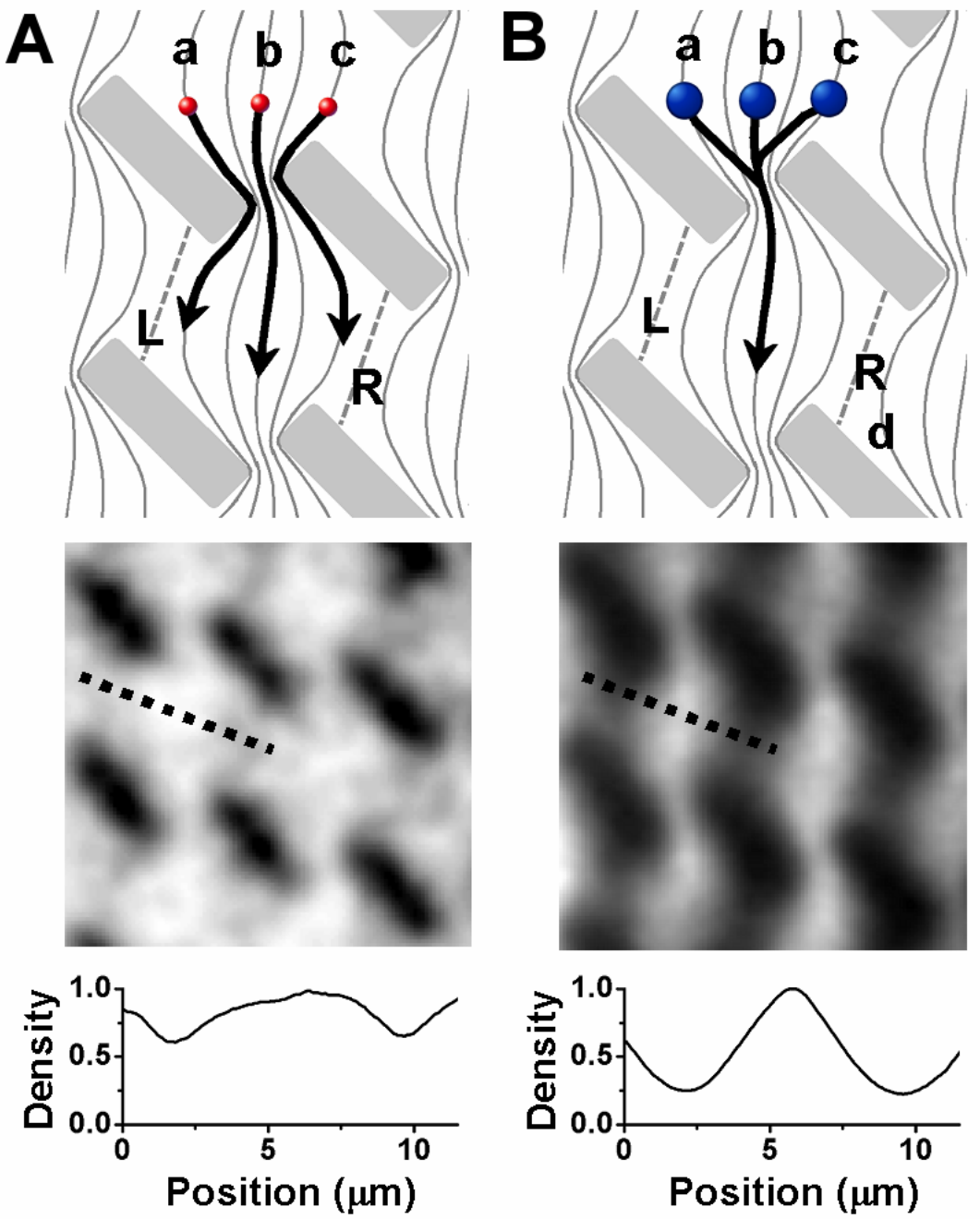

Fig. 2.5. Schematic flow diagram and fluorescence image of particles in the center of the band for particles of size (A) 411 b at average flow speed of 250 μm/s and (B) 48.5 kb (2 μm/s). The exposure time was long enough to show the particle density. The lower two images show brightness (normalized molecule density) vs. position along the dotted lines of the fluorescent images.

We believe that the reason the array failed to deflect small molecules (411 b DNA) lies in the fact that small particles can precisely follow the electric field lines as they flow through the obstacle geometries (Fig. 2.5A). Contrary to the basic principles of the diffusion array [3, 4], where particles could widen out over the parabolic shaded region in fig. 2.1 only via diffusion, small molecules will be spread out by the electric field. Particles now drift towards the vicinity of boundary *L* (via field line *a* in Fig. 2.5A) as well as to the boundary *R* (via field line *c*). Therefore point-like particles are equally likely to diffuse in both directions [8]. Here is the mathematically strict argument. For small particles that precisely follow electric field lines, their flux density $J_{particle}$ can be written as $J_{particle} = \rho\mu E - D\nabla\rho$, where ρ is the particle density, μ is the mobility, and D is the diffusion coefficient. The first term of the flux density is due to the electric field, whereas the second term is from diffusion. According to the continuity equation, we have:

$$-\frac{\partial\rho}{\partial t} = \nabla\bullet J_{particle} = \mu E\bullet\nabla\rho - D\nabla^2\rho \tag{2.5}$$

Note we have used $\nabla\bullet E = 0$ because the electrolytic solution is neutral. If there is a high field, so that the second term in Eq. 2.5 becomes relatively small, we find at steady-state:

$$E\bullet\nabla\rho = 0. \tag{2.6}$$

This says the particle density is approximately constant along any field line. Thus if one has a uniform concentration of particles arriving across all field lines entering a given gap (originating from a reservoir of uniform concentration), as the field lines (particle streamlines) widen out after the gap, the particle density will remain unchanged. This is illustrated in the fluorescence image of 411 b DNA molecules in the array (Fig. 2.5A), which shows that DNA under high fields uniformly fills the entire space between rows of

obstacles. Now, consider uniform injection of particles into all gaps at the top of the array using high fields, leading to uniform particle distribution in the array, and then we lower the field strength so that diffusion becomes important. Since all spatial derivatives of ρ in Eq. 2.5 are zero in our case of uniform density distribution, the particle density stays uniform according to Eq. 2.5, and thus the diffusion flux of particles across any field line must be equal to the inverse flux. Combined with translational symmetry, this implies that the probability of a particle diffusing across boundary *L* in Fig. 2.5A equals that across boundary *R*, a result which must hold for any distribution, not just for the assumed uniform distribution of particles. Given that there is no preferred direction of diffusion, there is no physical basis for ratcheting.

When a much larger λ DNA molecule approaches a gap, it is physically deflected by the obstacle and centered on the gap, because of its finite size (a random coil of ~1 μm) compared to the gap width (~1.4 μm). Thus molecules initially following field lines *a*, *b*, and *c* in Fig. 2.5B will all tend to leave the gap region on line *b*. The fluorescence image in Fig. 2.5B clearly shows this shadowing in contrast to Fig. 2.5A for the case of small molecules. Unlike 411 b molecules, which are spread out in the space between rows of obstacles by the field, λ DNA molecules can only reach boundaries *L* and *R* in Fig. 2.5B by diffusion. Because boundary *R* is farther than boundary *L* from the gap where molecules emerge, molecules are more likely to diffuse across boundary *R*. Once a molecule reaches field line *d*, it will drift to the right. Therefore the obstacle array acts as a Brownian ratchet.

2.7 Summary

Stable flows of precise direction and microscopic sample injection allowed for the realization of Brownian ratchet arrays. Flow directions were controlled using a long-and-narrow array design, with equipotential matching at the array edges and microfluidic channels acting as electrical current sources. Microfluidic channels connecting to different reservoirs enabled precise sample injection, which is necessary for detecting the small ratcheting effects. 48.5 kb from 164 kb DNA molecules were continuously separated using a 12 mm-long ratchet array, with a resolution of 1.4 and a running time of 2 hr.

This chapter clearly describes that there exists a critical particle size threshold, which is related to the size of the narrowest feature through which the particles must pass in the array [8]. Particles below this threshold maintain their flow along electric field lines through the gaps and are thus incapable of being ratcheted. Particles above this threshold size will be deflected from their original field lines by the obstacles, and can thus be ratcheted. Once above this size, larger particles are ratcheted less because of their lower diffusion coefficients. This points to the importance of very narrow gaps in the obstacle array if the separation of small particles is desired.

References

1. Feynman, R. P.; Leighton, R. B.; Sands, M. *The Feynman Lectures On Physics* Ch. 46 **Vol. 1** (Addison-Wesley, Reading, Massachusetts, 1966).
2. Astumian, R. D. *Science* **1997**, *276*, 917–922.
3. T. A. Duke, R. H. Austin, Phys. Rev. Lett. **80**, 1552 (1998).
4. D. Ertas, phys. Rev. Lett. **80**, 1548 (1998).
5. C. F. Chou, O. Bakajin, S. Turner, T. Duke, S. S. Chan, E. C. Cox, H. G. Craighead, and R. H. Austin, "Sorting by Diffusion: An Asymmetric Obstacle Course for Continuous Molecular Separation", *Proc. Natl. Acad. Sci.* USA **96** (24): 13762 (1999).
6. A. Oudenaarden and S. G. Boxer, "Brownian Ratchets: Molecular Separations in Lipid Bilayers Supported on Patterned Arrays ", *Science* **285**, 1046 (1999).
7. M. Cabodi, Y. F. Chen, S. W. P. Turner, H. G. Craighead, and R. H. Austin, *Electrophoresis* **23**, 3496.
8. Huang, L. R.; Silberzan, P; Tegenfeldt, J. O.; Cox, E. C.; Sturm, J. C.; Austin, R. H.; Craighead H. *Phys. Rev. Lett.* **2002**, *89*, 178301–178304.
9. Huang, L. R.; Tegenfeldt, J. O.; Kraeft, J. J.; Sturm, J. C.; Austin, R. H.; Cox, E. C. *International Electron Devices Meeting Technical Digest* **2001**, 363–366.
10. Volkmuth, W. D.; Austin, R. H. *Nature* **1992**, *358*, 600–602.
11. E. W. Becker *et. al*., Microelectronic Engineering 4 (1986), pages 35 to 56.
12. H. Becker *et. al*., J. Micromech. Microeng. 8 (1998), pages 24 to 28.

Chapter 3

Enhancing Separation Speed and Resolution of Brownian Ratchets by Flow Tilting

3.1 Basic Principles

This chapter presents an effective method for optimizing Brownian ratchet arrays [1]. The key parameter for optimizing an array of a given array geometry is the angle of the flow with respect to the array. The separation speed and resolution of the ratchet structure described in the previous chapter was improved by an order of magnitude using this flow tilting method.

Before optimization (Fig. 3.1A), the Brownian ratchet array was not useful because of its slow running speed [2–9]. Separation of DNA molecules can be improved dramatically by tilting the electrophoretic flow relative to the vertical axis of the array (Fig. 3.1B) [1]. This improvement occurs because for the same amount of diffusion, the probability that a molecule will be deflected is greatly increased compared to the case where the flow is aligned to the vertical array axis, as it is in Fig. 3.1A.

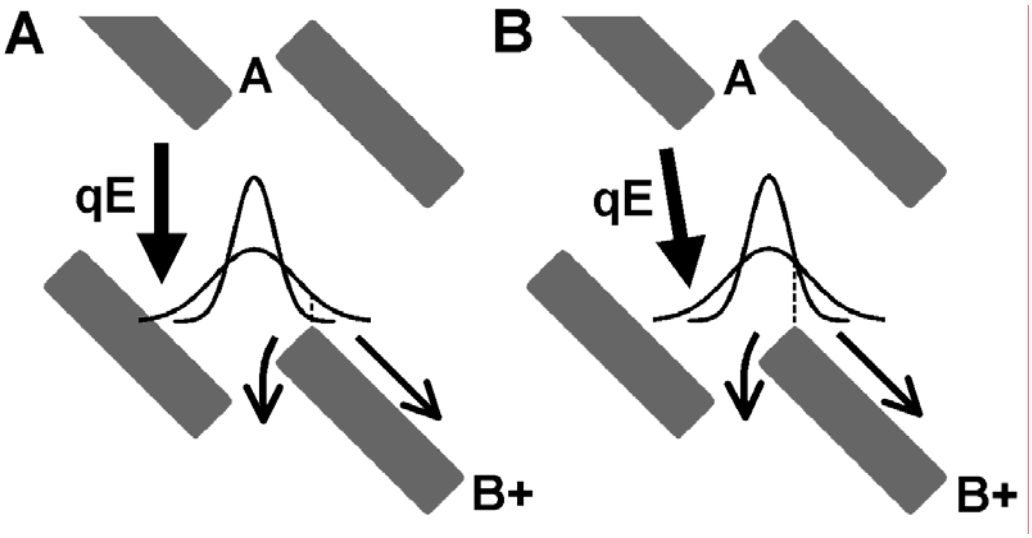

Fig. 3.1. Basic principle of the flow tilting. Particles are driven through the array hydrodynamically or electrophoretically (pictured). (A) Particles of different sizes diffuse to different extents (bell-shaped curves represent lateral distributions of small and large particles) resulting in different probabilities of deflection to B+. The vertical dotted line within the distributions represents the required diffusion for ratcheting to gap B+. (B) The probability of a particle being deflected to B+ is increased by tilting the flow at a small angle with respect to the vertical axis of the array.

3.2 Device Design

The focus of this optimization method is not to vary the array geometry, but rather to tilt the flow, which turns out to be an effective method for enhancing the performance of ratchets with a given array geometry. The direction of electrophoretic flow, carried by ions in the fluid, is tilted with respect to the vertical array axis by a small angle θ_{tilt}. Three features are incorporated in the device design to control the average current direction and create straight bands of molecules throughout the array (Fig. 3.2):

(i) To create the correct boundary condition at the top and bottom of the array, the top and bottom edges are slanted at an angle, chosen to set the

edges along equipotential lines determined by numerically solving the Laplace equation for the array geometry for each θ_{tilt} [9].

(ii) Microfluidic channels leading into the array act as electrical resistors each one of which will carry approximately the same amount of current. The resistance of their parallel combination is large compared to the sheet resistance of the array. This reduces any residual distortion of the current distribution near the top and bottom edges [10].

(iii) The array is long and narrow (13 mm by 3 mm) and essentially one dimensional, with flow lines parallel to the side edges. This feature is new compared to the previous device with no flow tilting.

Individual arrays were made for θ_{tilt} of 3.6^{o}, 7.2^{o} and 10.8^{o}.

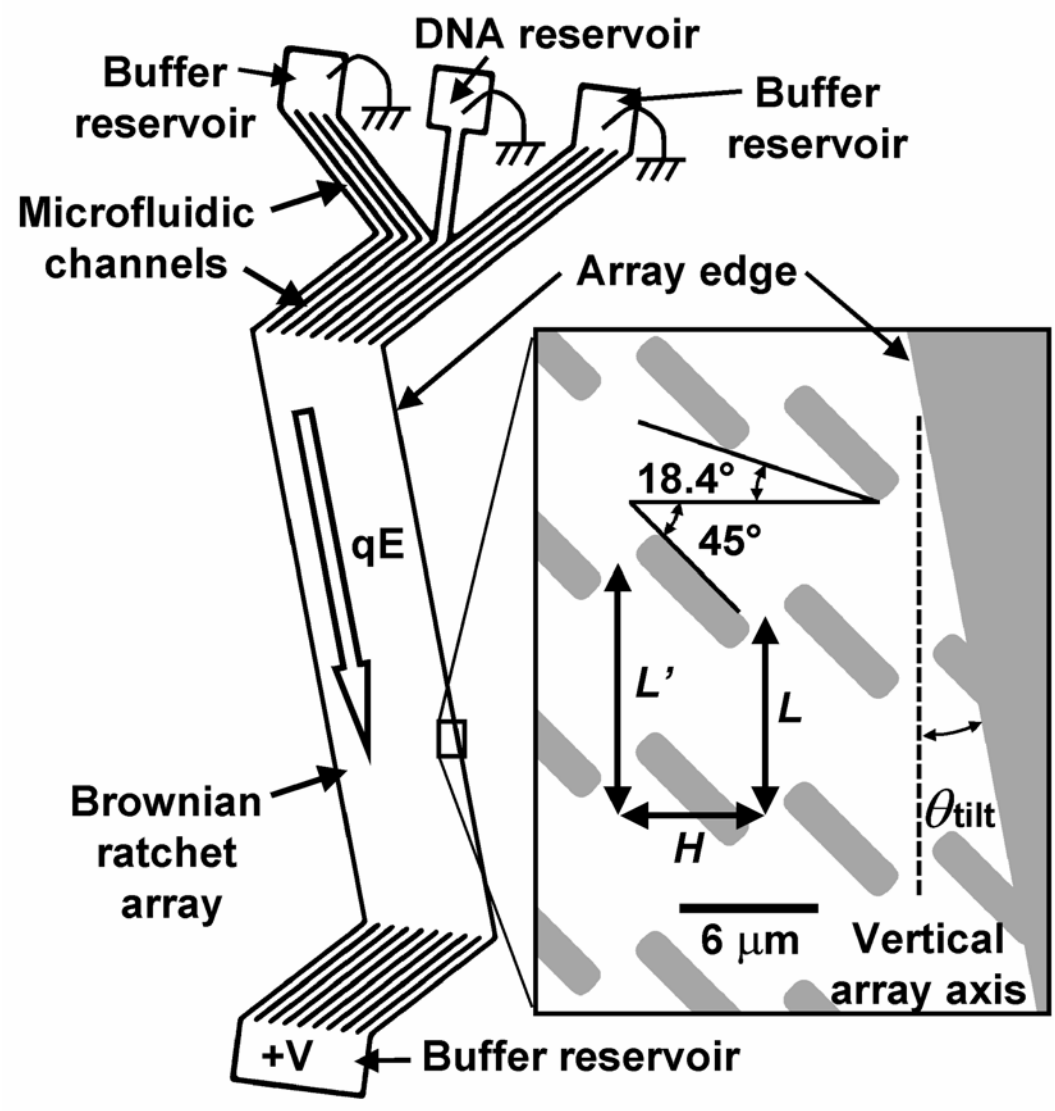

Fig. 3.2. Schematic diagram of the device at the flow angle of θ_{tilt} = 10.8^o with respect to the vertical array axis. Devices of θ_{tilt} = 3.6^o and 7.2^o were identical except for θ_{tilt}. The pitch of the columns of obstacles, the vertical pitch of the rows, and the vertical distance from gap A to gap B+ (Fig. 1A)—defined as *H*, *L* and *L'*, respectively—were 6 μm, 8 μm and 10 μm respectively in our experiments. The obstacles were ~5.6 μm long, ~1.4 μm wide, and ~3.2 μm tall.

3.3 Optimum Flow-Tilt Angle

Fig. 3.3 shows separation of coliphage λ DNA (48.5 kb, ~5 μg/ml) and coliphage T2 DNA (164 kb, ~2 μg/ml) when the ion flow was applied at 7.2^o with respect to the vertical array axis ($\theta_{tilt} = 7.2^o$, velocity ~1.5 μm/s). The deflection of the 48.5 kb DNA was greatly increased from the previous case (Fig. 2.4B), where $\theta_{tilt} = 0$, and even the 164 kb molecules were somewhat deflected from the vertical direction. This can be qualitatively understood from Fig. 3.1B, which shows that the fraction of transversely diffusing molecules captured by the ratchet is increased by tilting the direction of ion flows. Most significantly, the separation angle (defined as the angle between the two bands) has now increased from 1.3^o at $\theta_{tilt} = 0^o$ to 6.3^o at $\theta_{tilt} = 7.2^o$ and the resolution between the two peaks from ~1.4 to ~4.1 at 11 mm from the injection point. Fig. 3.3B shows the electrophoretograms under these conditions measured at 3 mm, 6 mm, 9 mm and 12 mm from the top of the array.

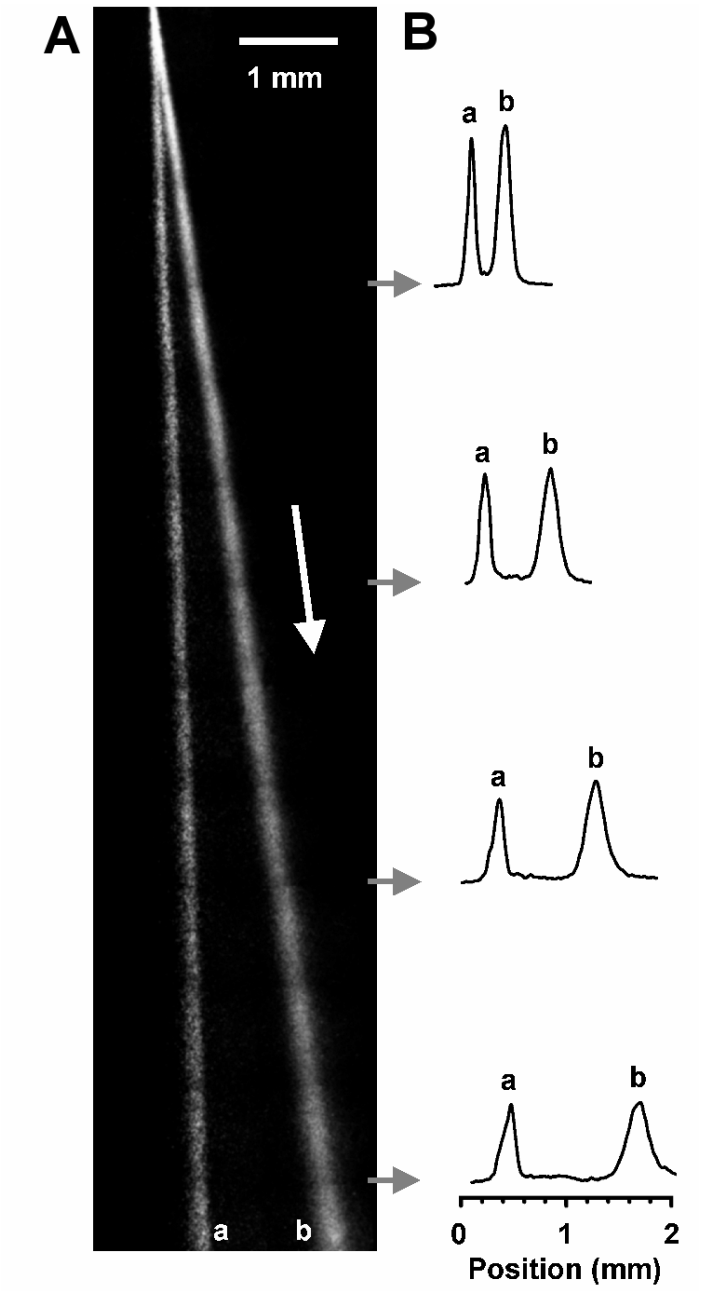

Fig. 3.3. Fluorescent micrograph of 48.5 kb and 164 kb DNA in Brownian ratchet arrays. The molecules were injected at a single point at the top of the array. (A) Tilted flow (θ_{tilt} = 7.2^o) at ~1.5 μm/s. The arrow shows the direction of the ionic flow θ_{tilt}. Band assignment for DNA: (a) 164 kb; (b) 48.5 kb. (B) Electrophoretograms of (A) measured at 3 mm, 6 mm, 9 mm and 12 mm from the injection point.

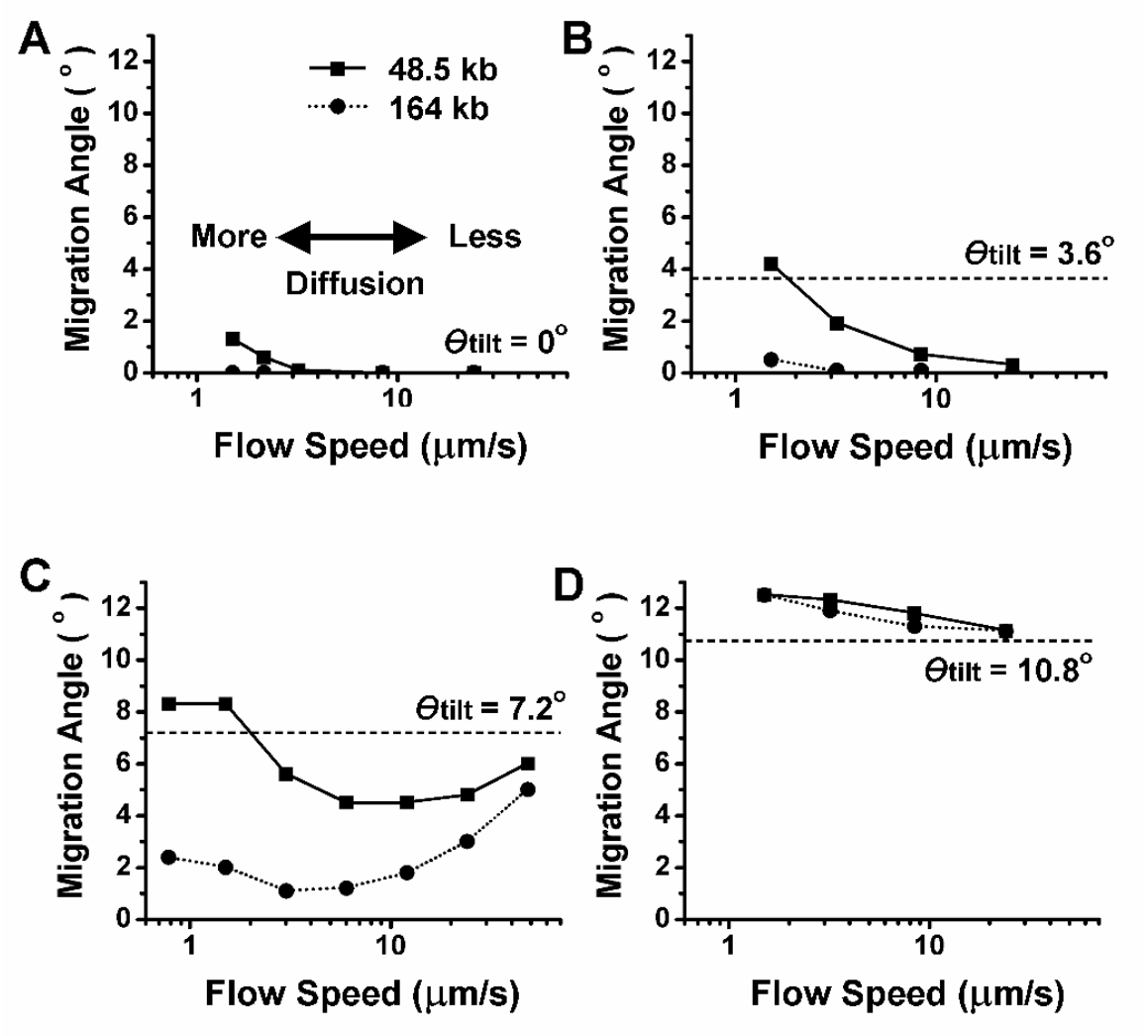

Fig. 3.4. Measured migration angles of DNA molecules as functions of flow speed, at (A) zero ion flow angle ($\theta_{tilt} = 0^o$) (B) $\theta_{tilt} = 3.6^o$ (C) $\theta_{tilt} = 7.2^o$ and (D) $\theta_{tilt} = 10.8^o$. For comparison, the dotted horizontal lines show θ_{tilt}. Lower speed allows for more diffusion and more ratcheting.

The migration direction of a molecule with respect to the vertical array axis (defined as migration angle θ_{mig}) is plotted as a function of DNA flow speed for flow angles (θ_{tilt}) of 0^o, 3.6^o, 7.2^o and 10.8^o in Fig. 3.4. Also shown schematically (dotted lines) in each panel is the tilt angle of ion flow (θ_{tilt}) with respect to the vertical array axis. As expected, the migration angles at a tilt of 3.6^o are greater than those for no tilt ($\theta_{tilt} = 0^o$), and they decrease at higher flow speeds, again because there is insufficient time for diffusion. At $\theta_{tilt} = 7.2^o$, the migration angles and separation are larger still, and the migration angles decrease as expected with flow speeds up to about 6 μm/s. At larger speeds, surprisingly, they increase again. To understand this behavior, we have to consider the detailed flow distribution in the array.

Fig. 3.5 shows the computer-simulated electric field lines in the array. The basic idea illustrated in Fig. 3.1B is still valid, even though we had assumed that the detailed flow distribution was uniform. Compared to Fig. 3.5A, where $\theta_{tilt} = 0^o$, Fig. 3.5B shows that the diffusion distance required to trigger a ratcheting event is reduced when $\theta_{tilt} = 7.2^o$. Therefore, molecules have a higher probability of being ratcheted, which is the basic idea illustrated in Fig. 3.1B.

3.4 Role of Molecular Size and Stretching

We believe that at $\theta_{tilt} = 7.2^o$, the migration angles go up as we increase the flow speed up, is because DNA elongates and reptates at high fields, and thus has a smaller

cross section, behaving like a smaller particle as it passes through the gaps (Fig. 3.5C). The DNA then is not subject to ratcheting, but follows the direction of ion flow. At a tilt of 10.8°, both large and small molecules migrate at a similar large angle, independent of flow speeds, with little separation. We believe that this occurs because we are beginning to approach the critical tilt condition (~18° in our case) at which half of the flow lines would be diverted to the adjacent gap solely by the tilt, independent of diffusion. This would lead to a breakdown of ratcheting. In any case, data for this array geometry shows that the optimum angle θ_{tilt} for separation is ~7°.

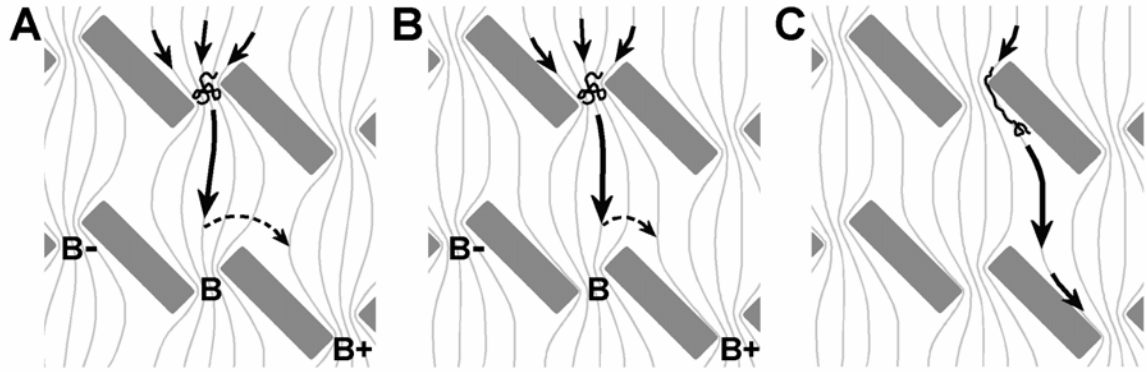

Fig. 3.5. Computer-simulated electric field lines in the array. (A) Zero flow angle (θ_{tilt} = 0°). Dashed arrow shows the required Brownian motion for a molecule to be deflected to B+. (B) θ_{tilt} = 7.2°. Less Brownian motion is required for deflection. (C) DNA molecules, stretched at high flow speed, tend to follow single field lines and thus the flow direction.

3.5 Resolution as a Function of Flow Speed

Fig. 3.6 shows the dependence of resolution on flow speed at θ_{tilt} = 7.2°. The resolution of the two bands is defined as $\Delta X / (2\sigma_1 + 2\sigma_2)$ to measure the peak separation

ΔX relative to the full bandwidths ($2\sigma_1$ and $2\sigma_2$) [12]. As expected, at high flow speeds the resolution decreases because of insufficient time for diffusion. At very low speeds, however, resolution decreases again, this time due to excessive diffusion, leading to band broadening.

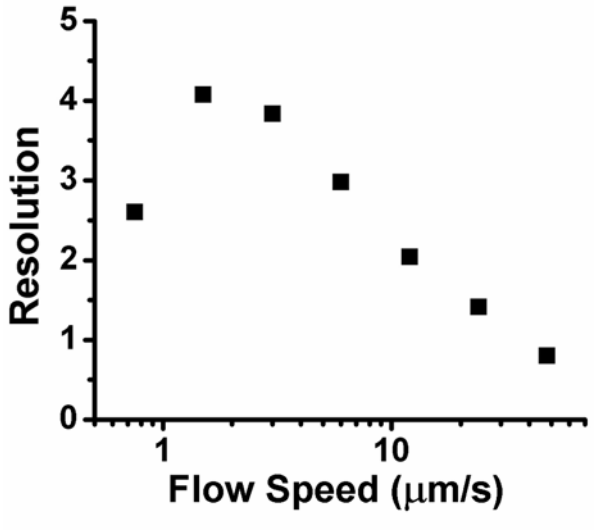

Fig. 3.6 Resolution of 48.5 kb and 164 kb molecules at θ_{tilt} = 7.2° and various flow speeds measured 12 mm from the injection point.

3.6 Modeling of Band Broadening

The rate of band broadening is important because it affects the resolution with which molecules of different sizes can be separated. Band broadening in a ratchet array should follow a binomial distribution [11], because the positions of molecules are reset to the centers of the gaps every time they pass through the gaps [4, 9]. Therefore, each ratcheting event is statistically independent, and both the migration angle θ_{mig} and band

broadening should depend on a single parameter, p, the probability of a molecule being deflected after one row of obstacles [4, 5]. According to the geometry of the array (Fig. 3.2, inset), a molecule will shift a distance H horizontally and L' vertically if deflected, or a distance L if it is not deflected. Therefore, the average displacement after one row of obstacles is Hp horizontally, and $L(1–p) + L'p$ vertically; the average migration angle θ_{mig} is

$$\theta_{mig} = tan^{-1}(Hp/[L(1–p) + L'p]),$$

and when p is small, we can approximate it as

$$\theta_{mig} = (H/L)\, p,$$

or equivalently

$$p = (L/H)\ \theta_{mig}. \tag{3.1}$$

This equation allows one to extract the parameter p from the experimentally-measured migration angle θ_{mig}. The half bandwidth (standard deviation) σ of this binomial distribution after N rows of obstacles, is

$$\sigma^2 = \sigma_o{}^2 + H^2\, Np(1–p), \tag{3.2}$$

where σ_o is the initial half-width (standard deviation). For our choice of H, L and L' (6 μm, 8 μm and 10 μm, respectively), Eq. 3.1 and 3.2 reduce to

$$p = 4/3\ \theta_{mig} \tag{3.3}$$

and

$$\sigma^2 = \sigma_o{}^2 + (16\ \mu m^2) N\theta_{mig}(3 – 4\theta_{mig}),$$

respectively. For a given vertical distance y from the injection point, we have $N = y/[L(1–p) + L'p]$, or $N = y/[(1–p)\ (8\ \mu m) + p\ (10\ \mu m)]$ in our case. p is small by assumption, and thus we substitute $y/(8\ \mu m)$ for N and get

$$\sigma^2 = \sigma_o^{\,2} + (2\ \mu\text{m}) y \theta_{\text{mig}}(3 - 4\theta_{\text{mig}}). \qquad (3.4)$$

This equation predicts the bandwidth according to the migration angle θ_{mig}.

We now compare the theoretical predictions of bandwidths using Eq. 3.4 to the data. For a speed of ~1.5 μm/s, the migration angles θ_{mig} and extracted ratchet probabilities p for 48.5 and 164 kb DNA were ~8.3° and ~2.0° and ~0.19 and ~0.05, respectively. The initial bandwidth (2σ) was ~53 μm. At the end of the 12-mm array, the full widths of the two bands had grown to ~195 μm and ~115 μm, respectively. Fig. 3.7A shows the observed and theoretical (Eq. 3.4) bandwidths as a function of position in the array, with no adjustable parameters used in the theory. Also shown for comparison are bandwidths (2σ) predicted by simple free diffusion of DNA in aqueous buffer, ignoring any effects of the obstacles, using diffusion constants from the literature (~0.64 $\mu m^2/s$ and ~0.28 $\mu m^2/s$ for 48.5 and 164 kb DNA, respectively) [13]. Clearly the agreement between the data and Eq. 3.4 is excellent, and free diffusion does not accurately model band broadening in our array. Similar excellent agreement between data and the ratcheting theory for a speed of 3.0 μm/s is shown in Fig. 3.7B.

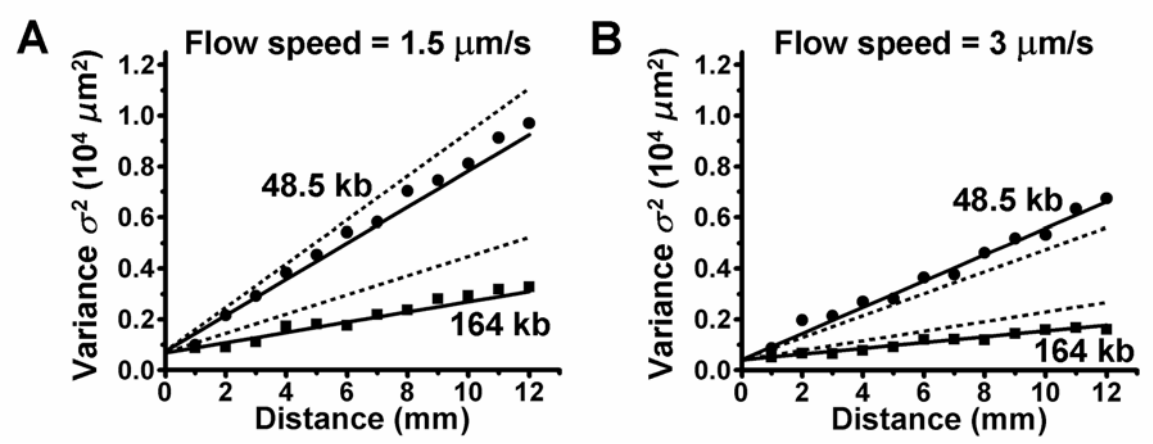

Fig. 3.7. Measured variance (half width squared, σ^2) of 48.5 kb (circles) and 164 kb (squares) molecules vs. distances from the injection point. Flow speeds were (A) ~1.5 μm/s and (B) ~3 μm/s respectively at θ_{tilt} = 7.2°. Solid lines are predictions from Eq. (3.4) using measured initial widths and migration angles (Fig. 4C). Dotted lines indicate band broadening expected from free diffusion alone.

With confidence in our model of band broadening, we can extrapolate our results to predict the performance of arrays longer than the 12-mm array presented in this chapter. Because the bandwidths increase with the square root of distance and the separation of the bands increases linearly, the resolution increases as the square root of the array length. At a tilt angle of θ_{tilt} = 7.2° and a DNA flow rate of ~3 μm/s, our 12 mm array (running time = ~70 min) achieves a resolution of ~3.8 between 48.5 kb and 164 kb molecules (Fig. 3.6), corresponding to the ability to resolve a 38% difference in molecular weight. Two peaks are resolved if the resolution is larger than 1. The percentage resolution R_p is calculated from the resolution R_s defined in Ref. 12 using the equation:

$$(1+ R_p) = (m_2 / m_1)^{(1/Rs)},$$

where m_2 and m_1 are molecular weights of the two peaks, and $m_2 > m_1$. In our case m_2 = 164 kb, m_1 = 48.5 kb and R_s = 3.8, we get R_p = 38%. To get R_p = 20%, the resolution R_s needs to be ~6.7 between m_2 and m_1, a factor of 1.76 larger than currently demonstrated (R_s ~ 3.8, using a 12 mm-long array). Therefore, the array should be about a factor of 1.76^2 longer to achieve R_p = 20%. Using the same conditions, a 37 mm-long array with a running time of 3 hr 40 min should resolve a 20% difference in the ~100 kb range. Conventional PFGE typically requires ~10 hr of running time to achieve similar resolution in this weight range.

3.7 Summary

This chapter shows that tilting the flow with respect to the array is an effective method for optimizing the ratchet performance for a given array geometry. The separation resolution and speed of the array were improved by a factor of 3 and 10 respectively, by tilting the flow at a small angle with respect to the array. Because the amount of diffusion required for ratcheting is greatly reduced, the separation is faster and the resolution is higher. A resolution of ~3.8 is achieved in ~70 min for 48.5 kb from 164 kb DNA molecules, using a 12 mm-long array with a flow tilt angle of 7.2^o. The band broadening scales with a binomial distribution model, which enables us to predict that the resolution improves with the square root of array length.

References

1. Huang, L. R.; Cox, E. C.; Sturm, J. C.; Austin, R. H., *"A Tilted Bownian Ratchet for DNA Analysis," Anal. Chem.* **2003**, accepted.
2. Feynman, R. P.; Leighton, R. B.; Sands, M. *The Feynman Lectures On Physics* Ch. 46 **Vol. 1** (Addison-Wesley, Reading, Massachusetts, 1966).
3. Astumian, R. D. *Science* **1997**, *276*, 917–922.
4. T. A. Duke, R. H. Austin, Phys. Rev. Lett. **80**, 1552 (1998).
5. D. Ertas, phys. Rev. Lett. **80**, 1548 (1998).
6. C. F. Chou, O. Bakajin, S. Turner, T. Duke, S. S. Chan, E. C. Cox, H. G. Craighead, and R. H. Austin, "Sorting by Diffusion: An Asymmetric Obstacle Course for Continuous Molecular Separation", *Proc. Natl. Acad. Sci.* USA **96** (24): 13762 (1999).
7. A. Oudenaarden and S. G. Boxer, "Brownian Ratchets: Molecular Separations in Lipid Bilayers Supported on Patterned Arrays ", *Science* **285**, 1046 (1999).
8. M. Cabodi, Y. F. Chen, S. W. P. Turner, H. G. Craighead, and R. H. Austin, *Electrophoresis* **23**, 3496.
9. Huang, L. R.; Silberzan, P; Tegenfeldt, J. O.; Cox, E. C.; Sturm, J. C.; Austin, R. H.; Craighead H. *Phys. Rev. Lett.* **2002**, *89*, 178301–178304.
10. Huang, L. R.; Tegenfeldt, J. O.; Kraeft, J. J.; Sturm, J. C.; Austin, R. H.; Cox, E. C. *International Electron Devices Meeting Technical Digest* **2001**, 363–366.
11. Feller, W. An Introduction to Probability Theory and Its Applications, 3rd ed. (Wiley, New York, 1967).
12. Giddings, J. C. *Unified Separation Science* p.101 (John Wiley & Sons, New York, 1991).
13. Nkodo, A. E.; Garnier, J. M.; Tinland, B.; Ren, H; Desruisseaux, C.; McCormick, L. C.; Drouin, G.; Slater, G. W. *Electrophoresis* **2001**, *22(12)*, 2424–2432.

Chapter 4

Microfluidic Tango Arrays for Separation without Dispersion

4.1 Introduction

Separation by size or mass is a fundamental analytical and preparative technique in biology, medicine, chemistry, and industry. Most conventional methods, including gel electrophoresis, field-flow fractionation, sedimentation and size exclusion chromatography are seriously compromised and ultimately defeated by the stochastic behavior of the material to be separated. For example, macromolecules of different sizes are usually separated by size exclusion chromatography (SEC), where a mixture is injected at one end of a tube packed with porous beads, and then washed through the tube (*1*). Molecules smaller than the pores can enter the beads, which lengthens their migration path, whereas those larger than the pores can only flow between the beads. In this way smaller molecules are on average retained longer and thus become separated from larger molecules. Zones broaden, however, as they pass through the column. This is because there are many possible migration paths for each molecule. Each path has a different length, and consequently a different retention time. This multipath zone broadening (Eddy diffusion) is a major factor limiting resolution (*2*). Other methods for

separation according to size, including gel electrophoresis and field-flow fractionation, also involve stochastic processes, which limit their resolution (*3*–*7*).

This need not be so. In this chapter we describe a separation process that approaches zero band broadening in the limit of high Peclet number, where Brownian motion is negligible. Peclet number (*Pe*) is defined as $\frac{vd}{D}$, where v is the flow speed, d is the characteristic dimension of the array, and D the diffusion coefficient of the particle being separated. We achieve these conditions experimentally by using high flow speeds. Depending on their sizes, particles in such flows either zigzag through the array or are channeled by the obstacles—the migration paths are predictable. We develop a theory for this approach, and have achieved continuous-flow sorting of ~1 μm diameter spheres with 10 nm resolution in 40 s using the approach. Band broadening caused by the transport process is under the detection limit of our characterization technique using the best mono-disperse polystyrene microspheres commercially available.

4.2 Basic Principles

The basic theory of the transport process is illustrated schematically in Fig. 4.1. A microfluidic channel is filled with a matrix of microfabricated obstacles (Fig. 4.1A). Each row of obstacles is shifted horizontally with respect to the previous row by $\Delta\lambda$, where λ is the center-to-center distance between the obstacles (Fig. 4.1B), and $\varepsilon = \Delta\lambda/\lambda$. To simplify the discussion, let us assume that ε equals 1/3. Particles to be separated are driven through the matrix by fluid flow. Because of the low Reynolds number in these

devices, the flow lines are laminar and deterministic—that is to say, there is no turbulence, and all inertial effects are negligible (*8*).

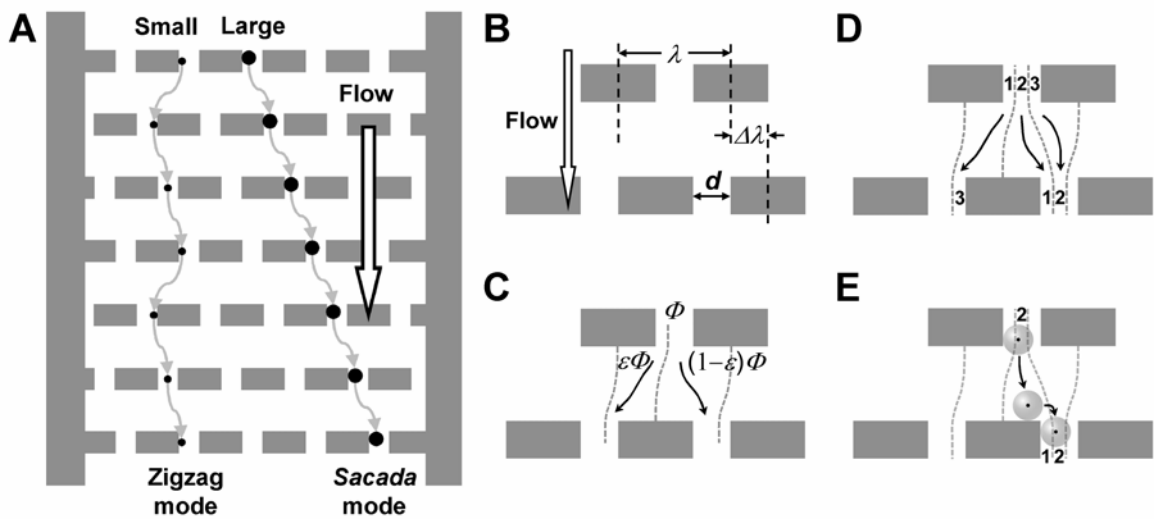

Fig. 4.1. Transport without dispersion. (A) Basic structure of a microfluidic channel filled with obstacles, where small particles migrate in the zigzag mode and large particles in the *sacada* mode. (B) Geometric parameters defining the obstacle matrix. (C) Bifurcation of fluid flows in the obstacle matrix. Dashed curves represent stagnant streamlines dividing the bifurcating flow. (D) Fluids from different relative positions (slots) flow to different slots in a predictable manner: slot 1 $\rightarrow$ slot 3 $\rightarrow$ slot 2 $\rightarrow$ slot 1. (E) Large particles are physically displaced by obstacles. The dots on the spheres represent the hydrodynamic centers-of-mass, which always fall in slot 2.

When the fluid emerging from a gap between two obstacles in one row encounters an obstacle shifted laterally by $\Delta\lambda$ in the next row, the fluid will divide and flow around the obstacle (Fig. 4.1C). For the average flow direction to be parallel to the walls of the channel, 1/3 of the total flux Φ will go to one side of the obstacle, and (2/3)Φ will go to the other side. Now let us divide each gap into three flow regions, which we will call slots, through each of which 1/3 of the total flux will move (Fig. 4.1D). By definition, all

streamlines from slot 1 will enter slot 3 in the next row. Similarly, flows from slot 2 will go to slot 1, and those from slot 3 to slot 2. The rule by which the relative positions change as fluids flow through different gaps is simple: slot 1 $\rightarrow$ slot 3 $\rightarrow$ slot 2 $\rightarrow$ slot 1, and so on.

Particles must follow streamlines—there are no inertial effects at low Reynolds number conditions—and thus they will flow periodically through slots 3, 2 and 1 as they move from gap to gap. Because of the "zigzag" motion of the particle, we will call this transport pattern the "zigzag mode," and zigzagging particles on average migrate along the flow direction defined by the sidewalls of the one-dimensional channel. Note that the path is not random, but deterministic and uniquely determined by the initial position.

In contrast, particles whose diameter is large compared to the slot width will not follow individual streamlines, but instead be propelled by many streamlines. This fundamentally changes their final migration direction. Fig. 4.1E shows a particle so large that its hydrodynamic center-of-mass falls in slot 2 when it is in contact with the obstacle wall next to slot 1. It is propelled by streamlines through slot 2, and thus approaches the next slot on track to move through slot 1, according to the rule established in the previous paragraph. The particle is, however, too big to fit into slot 1, and thus is physically displaced so that its hydrodynamic center-of-mass is once again in slot 2 (Fig. 4.1E). This process is repeated every time as a large particle approaches a row of obstacles, much as the *sacada* steps commonly used in the tango. We will thus call this transport pattern the "*sacada* mode." According to this theory, a particle's hydrodynamic radius

determines which transport mode it follows. Also note that the above argument can be easily generalized to electrophoresis by considering ion flows instead of fluid flows.

4.3 Device Design and Fabrication

We designed and constructed such a device (Fig. 4.2). The microfluidic channel is 16 mm long, 3.2 mm wide, and 10 μm deep. The matrix filling the channel consists of a square lattice of cylindrical obstacles (Fig. 4.2A), where the center-to-center distance, λ is 8 μm, and the spacing d between the obstacles 1.6 μm (Fig. 4.2B). The lattice is rotated by 5.7° (tan^{-1} 0.1) with respect to the channel (Fig. 4.2A), which defines the flow direction. The rotation of tan^{-1} 0.1 corresponds to $\varepsilon = 0.1$; thus a complete pitch λ is shifted every 10 rows (Fig. 4.2A). In principle, this configuration provides 10 slots, rather than the 3 discussed above. Particles are injected from a 10 μm-wide channel and carried across the matrix by a pressure-driven flow (*9*), which is made uniform by the many narrow channels on the top and bottom of the matrix (Fig. 4.2C). The microfluidic channels and the matrix were fabricated on a silicon wafer using photolithography and deep reactive ion etching, techniques conventionally used for silicon-based integrated circuit fabrication (*10, 11*). Holes through wafers for fluid access were drilled before sealing with a glass coverslip coated with silicone rubber (RTV-615 from General Electric) to form enclosed microfluidic channels.

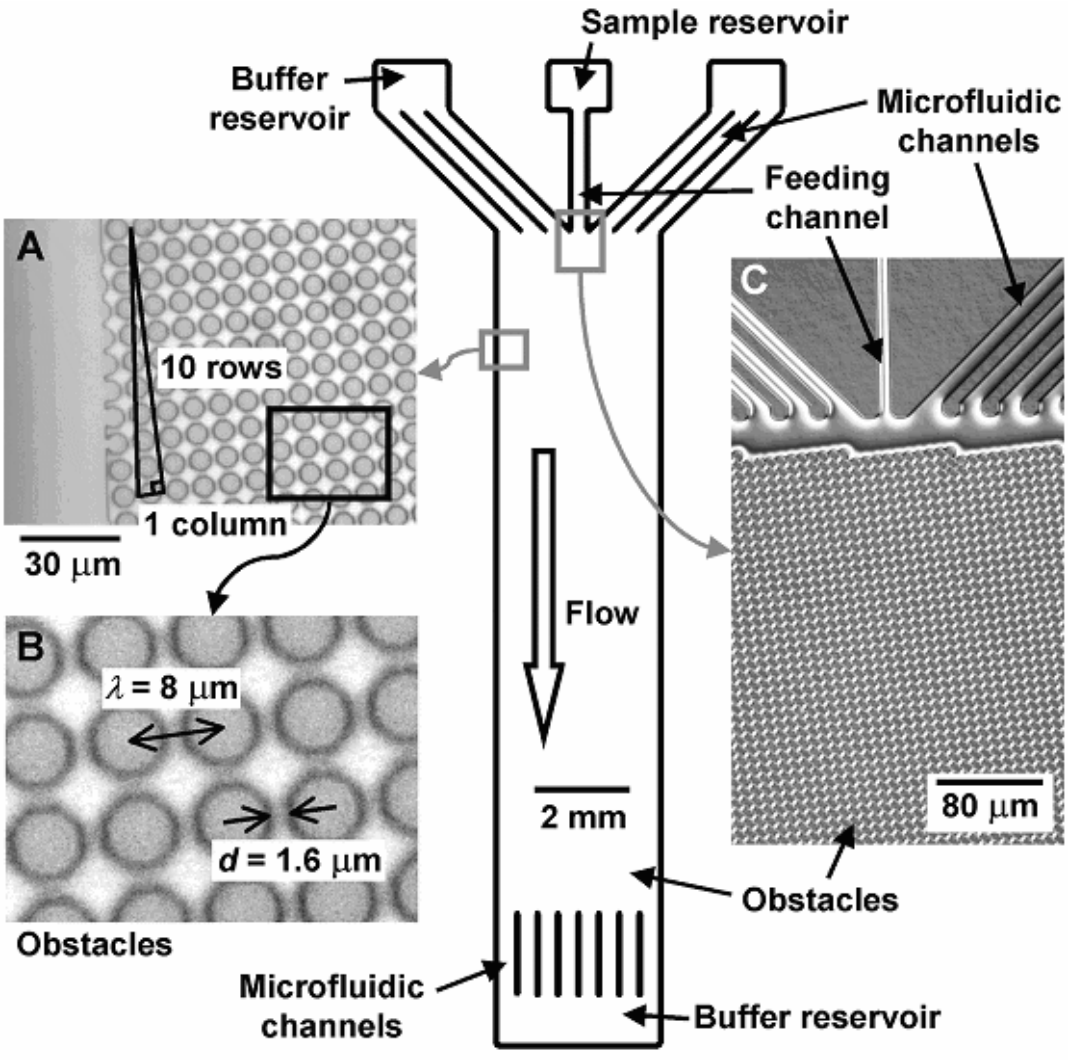

Fig. 4.2. Schematic diagram of a microfluidic device for continuous-flow separation.

4.4 Experimental Observation of Transport Modes

The two transport modes were experimentally observed using fluorescent polystyrene microspheres of 0.40 μm and 1.03 μm diameter in aqueous buffer (Fig. 4.3A). 0.1x Tris-Borate-EDTA buffer containing 0.02% POP-6, a performance-

optimized linear polyacrylamide (Perkin-Elmer Biosystems), was used in the experiments. The image was taken by fluorescent microscopy with a long exposure time to show trajectories of individual particles. The varying brightness along the trajectory reflects the different flow speeds of a microsphere in the matrix, dimmer in the narrow gaps due to higher flow speed and lower residence time. As predicted, the 0.40 μm microsphere (green) crossed a column of obstacles every 10 rows in the zigzag mode, whereas the 1.03 μm microsphere (red) was channeled along the axis of the obstacle array in the *sacada* mode.

Fig. 4.3B shows the continuous-flow separation of 0.40 μm and 1.03 μm microspheres injected into the matrix from a feed channel at the top. In this image many trajectories were superimposed. The 0.40 μm and 1.03 μm spheres migrated at ~0° (flow direction) and ~5.7° (matrix rotation) respectively relative to the flow direction, as expected. The pressure used to drive the flow was 30 kPa, which created an average flow speed of ~400 μm/s. The running time through the matrix was ~40 s.

4.5 Separation of Sub-Micrometer-Sized Polystyrene Beads

To probe the resolution of the device, fluorescent microspheres of 0.60 μm, 0.70 μm, 0.80 μm, 0.90 μm and 1.03 μm diameter were mixed and injected into the matrix. The concentrations of the microspheres of 0.60 μm, 0.70 μm, 0.80 μm, 0.90 μm and 1.03 μm were 0.015%, 0.010%, 0.010%, 0.005% and 0.005% solid, respectively. The beads were separated into different streams using a flow speed of ~40 μm/s, created by a

driving pressure of 3 kPa. The fluorescence profile scanned 11 mm from the injection point is shown in Fig. 4.4A. The measured migration directions with respect to the flow, defined as the migration angles, are plotted as a function of the microsphere size in Fig. 4.4B, which shows that under this flow speed (~40 μm/s), the transition from the zigzag to the *sacada* mode is gradual. The smooth transition is probably due to Brownian motion of the particles between streamlines, which we have ignored up to this point. At a flow speed of 40 μm/s, a 0.6 μm particle—diffusion coefficient in water of 0.73 $\mu m^2/s$ (*12*)—has a diffusion length of ~0.54 μm over the 0.2 s it takes to move the 8 μm from one row of obstacles to the next. This is a factor of 3 larger than the average slot width of ~0.16 μm. Thus it is not surprising that we observe a gradual change from zigzag mode to *sacada* mode as the particle size is varied.

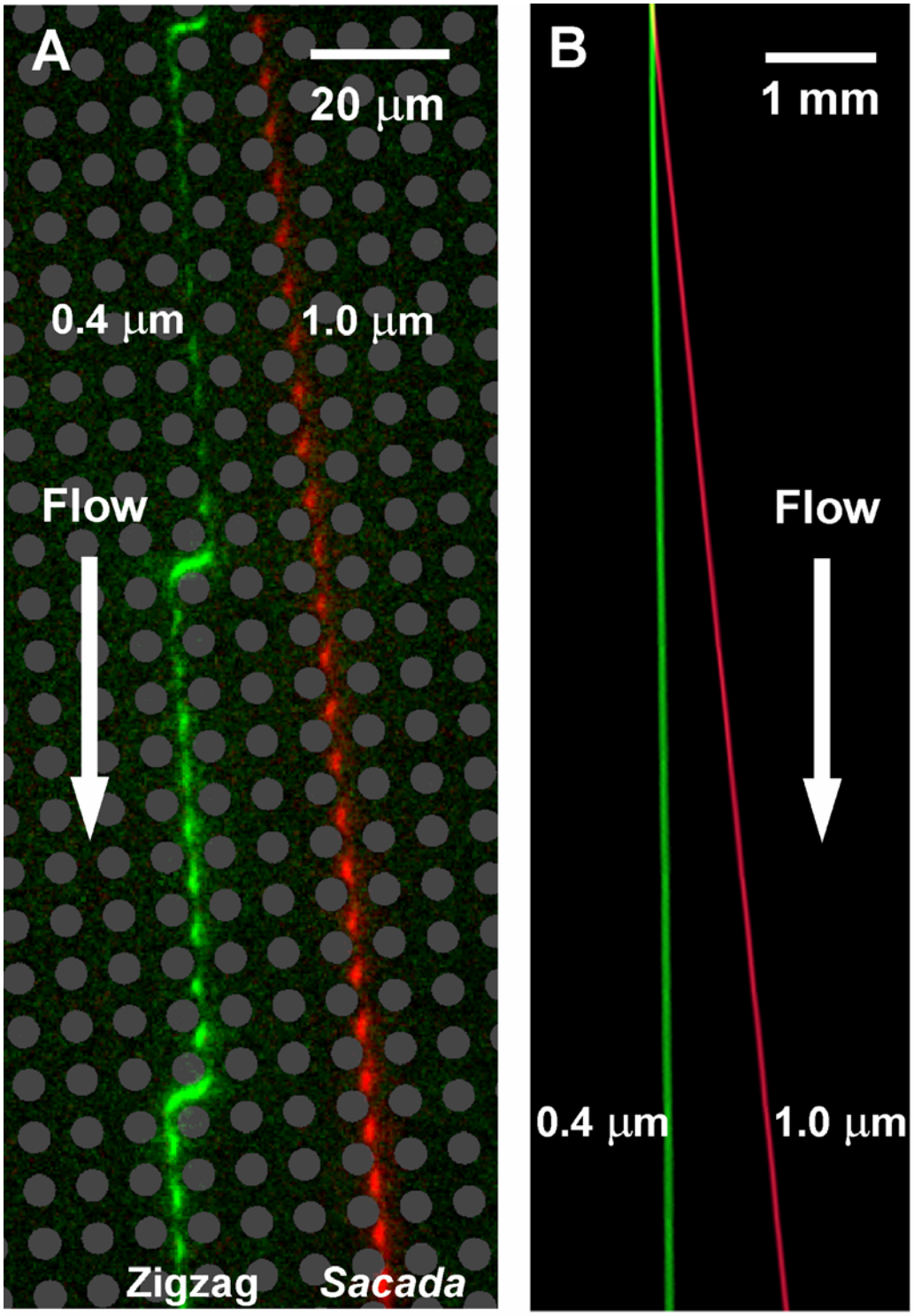

Fig. 4.3. Fluorescent images of microspheres migrating in the obstacle matrix, showing (A) the two transport modes for (B) the separation of microspheres with no dispersion. The gray dots in (A), which represent the obstacles, have been superimposed on the fluorescent image.

To minimize the effects of Brownian motion, the Peclet number was increased by increasing the flow speed. Fig. 4.4B shows a sharper transition when the flow speed is increased by a factor of 10 (~400 μm/s), created by a driving pressure of 30 kPa. The high flow speed not only increases the selectivity so that the device becomes more sensitive to size changes, but also shortens the running time to ~40s. The transition occurs at approximately 0.8 μm (Fig. 4.4B). The size coefficients of variation (*CV*) of the best monodispersed microspheres commercially available are 1.3%, 1.0% and 1.0% for 0.70 μm, 0.80 μm and 0.90 μm, respectively, as measured by the manufacturer. The peak widths measured at 11 mm from the injection point, correspond to *CV*'s of 2.5%, 1.2% and 0.9% for these three sizes, respectively (Fig. 4.4A). The coefficient of variation (*CV*) of particle diameter ϕ is defined as

$$\frac{\Delta\phi}{<\phi>} \times 100\%,$$

where $\Delta\phi$ is the standard deviation of ϕ, and $<\phi>$ the mean of ϕ.. Note that the measured peaks of 0.80 μm and 0.90 μm are as sharp as the size-variances of the microspheres themselves, and thus band broadening in our device is less than the known variance in particle size.

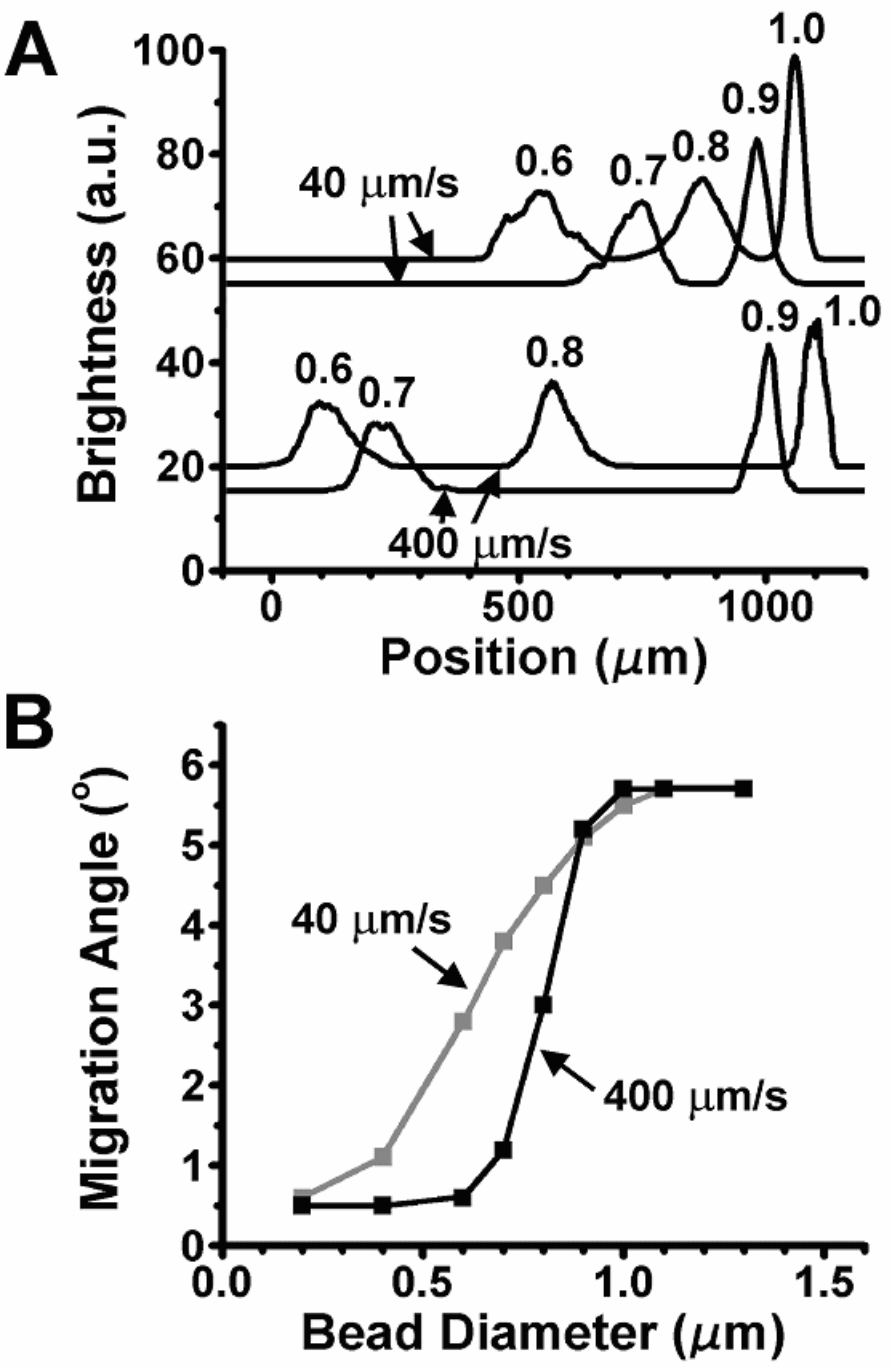

Fig. 4.4. (A) Fluorescent profiles of microspheres separated using flow speeds of ~40 μm/s (upper curves) and ~400 μm/s (lower curves) scanned at ~11 mm from the injection point. The 0.60 μm, 0.80 μm, and 1.03 μm diameter beads are green-fluorescent, while 0.70 μm and 0.90 μm are red, and thus each scan is shown as two curves representing the two colors. (B) Measured migration angles as a function of microsphere diameter at two different flow speeds.

4.6 Pore Size Chirping for High-Resolution Separation

One advantage of the flexibility of microfabrication is that the matrix can be designed to have varying gap widths as a function of distance, thereby optimizing separation for complex mixtures. To demonstrate this point, we fabricated a device containing 9 sections, each of which had a different gap width, starting with 1.4 μm and ending with 2.2 μm in increments of 0.1 μm (Fig. 4.5). The varying gap widths were designed to tune the critical diameter in 9 stages from ~0.70 μm to ~1.10 μm, so that a given sized particle would switch from one transport mode to the other as the gap size increased.

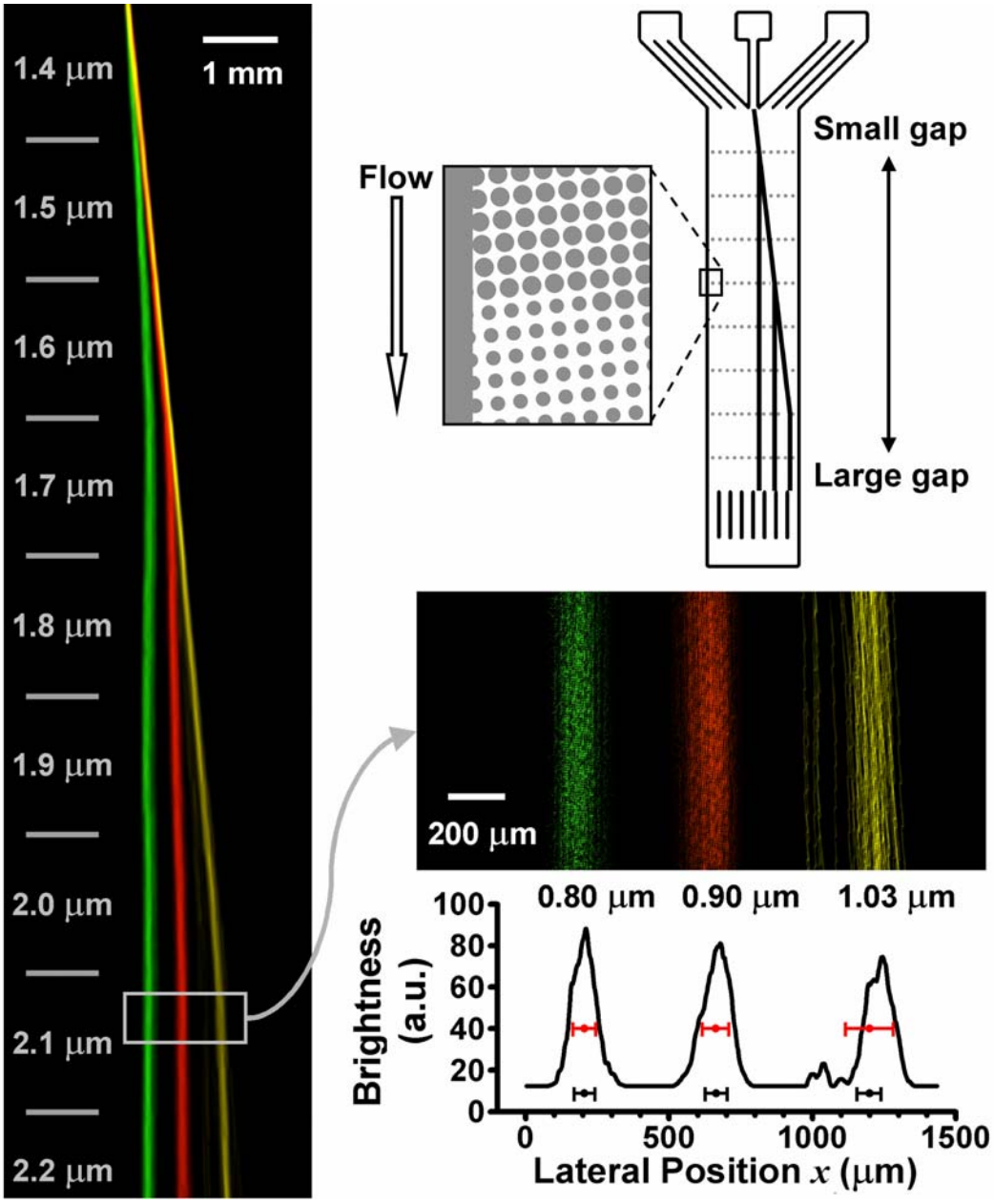

Fig. 4.5. High-resolution separation of fluorescent microspheres of 0.80 μm (green), 0.90 μm (red) and 1.03 μm (yellow), using a matrix of varying pore size. While the orientation and the lattice constants of the matrix are kept the same, the obstacle diameters are changed to creat`e different-sized spacings *d*, labeled on the left side of the fluorescent image. Individual 1.03 μm streamlines clearly show zigzag migration.

A mixture of monodisperse (*CV* = 1%) microspheres of 0.80 μm, 0.90 μm and 1.03 μm diameter was injected from the small-gap side of the matrix (Fig. 4.5), and flown at ~400 μm/s using a driving pressure of 30 kPa. Initially, all microspheres were larger than the critical size, and migrated at the same angle with respect to the vertical flow (*sacada* mode). Soon, however, the 0.80 μm microspheres (green) switched to the flow direction (vertical), presumably in zigzag mode. 0.90 μm microspheres switched to vertical at the fourth section, and the 1.03 μm microspheres made the transition around the eighth section. The fluorescent intensity profile was scanned at ~14 mm from the injection point (Fig. 4.5), and showed that the 0.80 μm, 0.90 μm and 1.03 μm peaks had *CV*'s of 1.1%, 1.2% and 1.9%, respectively (see the red scale bars, centered at the means of the peaks). By comparison, the 1% *CV* attributable to nonuniformity in the microsphere population is shown as the black scale bars underneath the peaks (*14*). Note that a fraction of the 1.03 μm microspheres were separated out from the main peak and formed a sub-band, most likely because of the non-homogeneity in the microsphere population. Again, the peaks are virtually resolved to the mono-dispersity of the most uniform microspheres commercially available. The running time was ~40 s.

4.7 Potential Methods for Improved Device Characterization

The results of Fig. 4.3 and 4.5 suggest that the resolution of the device may exceed our ability to measure it. One could in principle discover the limits of resolution for the approach by exploring the resolving power of the current array with a series of size classes varying in approximately 0.01 μm intervals around ~1 μm, each class with a

CV of ~0.1%. This is a demanding particle size requirement. DNA sequences are known with this and much higher accuracy, and in any size range, but due to the stochastic nature of these molecules, they become deformed randomly under the high shear conditions used here. Perhaps icosahedral viruses, whose symmetry and space group place stringent size limits on both the diameter of the particle and the size of the encapsulated genome, are ideal test objects, since there are many such viruses available and they span a range of sizes suited to the device.

Apart from the potential use of viruses to examine the resolution of our current device, we believe it can be used to fractionate and perhaps even identify viral particles, an identification that might be based purely on mass. For viruses below ~500 nm in diameter, the spacing of the obstacles in the array will have to be reduced, but not below the limits of optical lithography. For size fractionation and characterization of cell organelles and proteins, for which these arrays would appear to be ideally suited—equivalent in many ways to analytical ultracentrifugation but very much faster and cheaper—nano scale features will be required.

4.8 Summary

We have developed and tested a new technique for separation according to size, based on two deterministic transport modes, using a microfabricated matrix oriented at a small angle with respect to a driving flow. High flow speed increased the resolving power by reducing the effect of Brownian motion, and one percent difference in particle

size was routinely resolved in a running time of 40s. The ultimate resolution of the technique, in the light of real world issues such as statistical variations in the gap sizes, has yet to be established. With the use of finer lithographic tools, we expect that the method could be scaled to separate macromolecules and supramacromolecular assemblies with great analytical precision.

References

1. J. C. Giddings, *Unified Separation Science* (Wiley, New York, 1991).
2. J. C. Giddings, *Nature* **184**, 357 (1959).
3. J. C. Giddings, *Science* **260**, 1456 (1993).
4. L. R. Huang *et al.*, *Phys. Rev. Lett.* **89**, 178301 (2002).
5. J. Han, H. G. Craighead, *Science* **288**, 1026 (2000).
6. L. R. Huang *et al.*, *Nat. Biotechnol.* **20**, 1048 (2002).
7. P. T. Korda, M. B. Taylor, D. G. Grier, *Phys. Rev. Lett.* **89**, 128301 (2002).
8. R. P. Feynman, R. B. Leighton, M. Sands, *The Feynman Lectures On Physics* (Addison-Wesley, Reading, Massachusetts, 1966) vol. 2, chap. 41.
9. Huang, L. R.; Tegenfeldt, J. O.; Kraeft, J. J.; Sturm, J. C.; Austin, R. H.; Cox, E. C. *International Electron Devices Meeting Technical Digest* 2001, 363–366.
10. E. W. Becker *et. al*., Microelectronic Engineering 4 (1986), pages 35 to 56.
11. H. Becker *et. al*., J. Micromech. Microeng. 8 (1998), pages 24 to 28.
12. H. C. Berg, *Random Walks in Biology* (Princeton University Press, New Jersey, 1993) p. 56.

Chapter 5

DNA Prism I: Generation of Tunable Uniform Electric Fields

5.1 Motivation

The analysis and fractionation of large DNA molecules plays a key role in many genome projects. Conventionally, acrylamide or agarose gel electrophoresis techniques are used to separate small DNA fragments (<40,000 base pairs) [1]. For fragments larger than ~40 kilo-base pairs (kb), migration through the gel becomes independent of molecular weight, and thus pulsed-field gel electrophoresis (PFGE) is used [2–6]. However, PFGE is extremely time-consuming, with running times of typically more than 10 hours, depending on the molecular weight range and the resolution required.

Micron-scale hexagonal arrays of posts have been shown to separate DNA molecules in the 100 kb range in a few seconds [7–10]. The device comprises a sieving matrix ~1 μm deep, and a narrow constriction (entropic barrier) for sample concentration and launching. Alternating electric pulses oriented 120° apart were created with two pairs of electrodes connecting directly to the edge of the array. However, because the device lacks proper methods for generation of tunable uniform electric fields, the electric

fields, which are used to separate DNA molecules, are severely distorted. This has limited the resolution and usefulness of the design.

The realization of the DNA prism described here relies on the current injection methods [13], a technique which allows for the generation of tunable uniform electric fields in large-area of microfluidic arrays. To appreciate the need for the current injection method, let us first understand the basic principles for the continuous-flow separation of large DNA using the DNA prism device.

5.2 Basic principles for DNA prism separation

When alternating electric pulses of different strengths or durations are applied at different angles to a hexagonally-packed array of micron-scale posts, DNA molecules migrate in different directions according to their molecular weights (Fig. 5.1). When an electric field is applied in one direction, molecules of all sizes migrate between the posts with similar mobility (Fig. 5.1A). However, as the field direction is switched 120° with respect to the previous one, all molecules backtrack through channels formed by the posts [7–9] (Fig. 5.1B). The smaller molecules reorient more quickly, and thus are separated from the longer ones at each change in field direction (Fig. 5.1C). Because the electric pulses in one direction are stronger or longer than those in the other direction, molecules migrate in different directions. This is the physical basis for prism separation. Note that the asymmetry in pulse strengths or durations is crucial for continuous-flow separation—if pulses have identical strengths and durations in both directions, DNA molecules move in the same direction with different mobilities, as they do in conventional pulsed field gel

electrophoresis. The experimental realization of the DNA prism relies on the ability to generate uniform electric fields across the sieving array area, and to tune the directions of such uniform electric fields, which will be the topic of the next section.

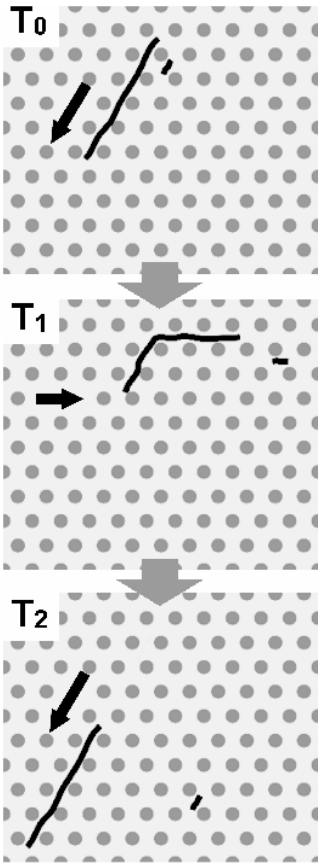

Fig. 5.1 Schematic showing the behavior of small and large DNA molecules in microfabricated arrays under a full cycle of asymmetric alternating-angle electric fields Arrows show the directions and speeds of DNA migration. (A) The high field moves both small and large molecules in a channel (arrow shows direction of motion). (B) A low field rotated 120^{o} causes reversal of the leading and trailing ends, and the low field (or short time) prevents the long molecule from sliding off the posts and reversing direction. (C) The original field reapplied. The ends again reverse, and the large molecule resumes its original track while the small molecule is now in a new track.

5.3 Conventional method for generation of tunable uniform electric fields

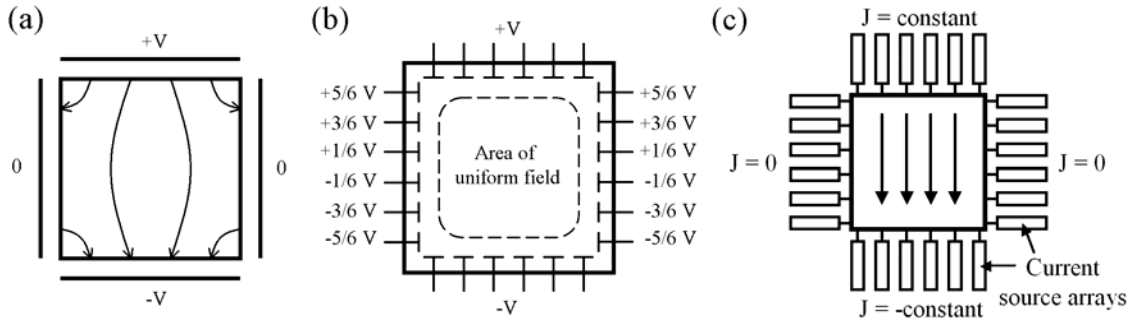

Fig. 5.2 (A) Highly nonuniform field generated by four electrodes. (B) Contour-clamped homogeneous electric field (CHEF) method, used in conventional PFGE apparatuses. (C) Current injection method.

To experimental implement the DNA prism, the ability to tune the direction of uniform electric fields rapidly have to be developed. In principle, one can use two pairs of electrodes to create tunable fields in a two-dimensional area (Fig. 5.2A), one pair for each field component (vertical or horizontal). However, the resulting field is highly distorted, because the electrodes perturb the field generated by one another. In conventional pulsed-field gel electrophoresis equipment, the problem is solved by using many electrodes to clamp the electric potential along a closed contour (Fig. 5.2B) [11]. Fundamentally, this is equivalent to imposing a Dirichlet boundary condition to the Laplace equation [12]. This "contour-clamped homogeneous electric field (CHEF)" method is inappropriate for microfluidic applications when the active array is only ~1cm x 1cm, however, because electrodes could interfere with other functions of a device, such as sample loading and extraction. It is also not very effective—even with the 24 electrodes typically used in commercial PFGE apparatuses, the field near the electrodes is

not uniform. Furthermore, microelectrodes inside fluidic channels are susceptible to erosion and bubble generation.

5.4 Current injection method

Here we describe a novel electrical current injection method, which is extremely useful for this microfluidic applications, because it

(i) requires no electrode inside the microfluidic channels,

(ii) incorporates structures for sample injection and extraction, and

(iii) most importantly, generates uniform fields over virtually the entire area of the array.

The current injection method uses the electric current injected on a closed contour, instead of the electric potential, to define the electric field (Fig. 5.2C). Because the medium inside the contour obeys Ohm's law, defining electric current perpendicular to the boundary is identical to defining the potential gradient (normal component) along the contour. Our use of thousands of current sources approximates Neumann boundary conditions (instead of Dirichlet boundary conditions), which uniquely determine the fields inside the boundary. In practice, current sources can just be resistors whose resistances are made high compared to that of the central array (Fig. 5.3A). Our device uses microfluidic channels fabricated on fused silica glass as the resistors. The channels connect the central array to a few buffer reservoirs, where voltage is applied through immersed contacts. The electrical resistances of the channels are controlled by their dimensions.

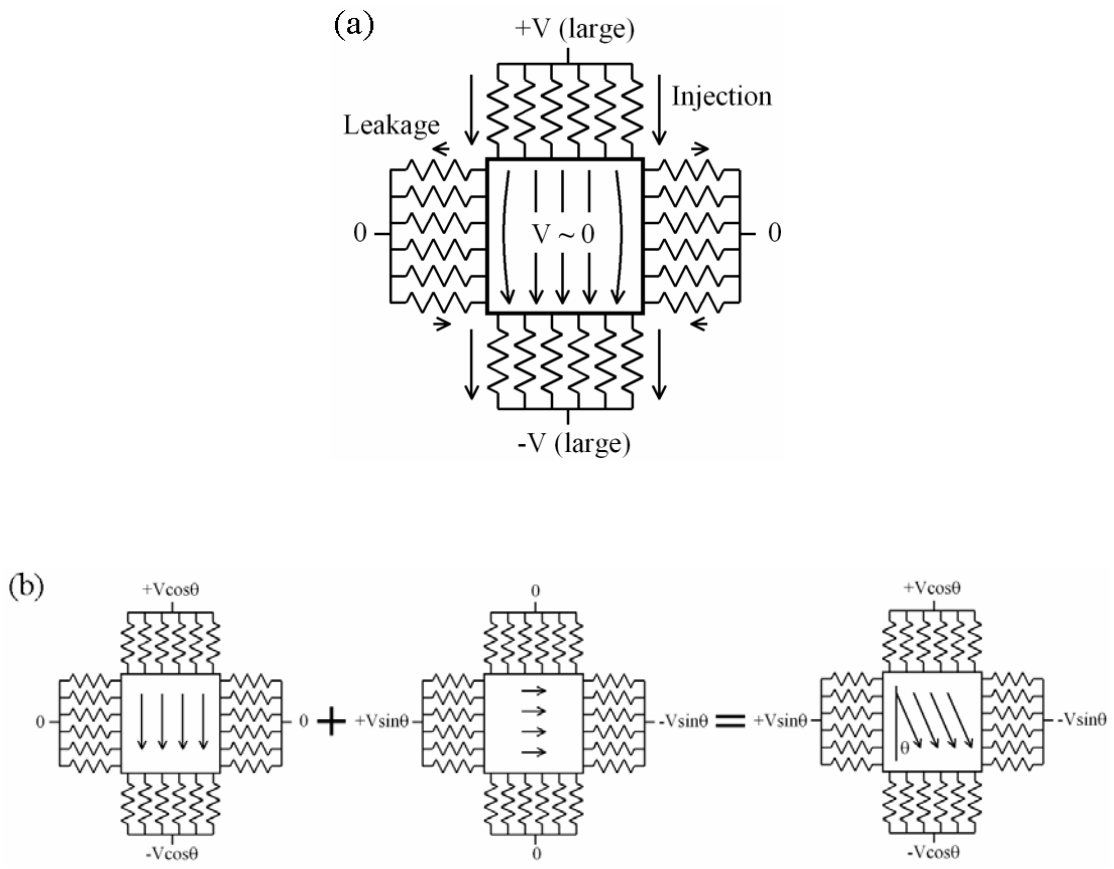

Fig 5.3 (A) Practical current injection with resistors. (B) Superposition principle for generating uniform fields at arbitrary directions. (θ is angle of field with respect to vertical).

Consider the field distribution in a square area surrounded by identical resistors (Fig. 2a). Because the resistances of the resistors are high, we have to apply a high voltage to drive current through the resistors. The injected vertical current from each resistor on the top is approximately the large voltage drop divided by its resistance, which to the first order is a constant. The current leakage through the resistors on the sides is, on the contrary, negligible because the voltage drop across the resistors is small. In the limit,

where the resistance approaches infinity, the field inside the square area will be perfectly uniform. Since horizontal fields can similarly be generated, fields at any orientation can be created using superposition of conditions for horizontal and vertical fields (Fig. 2b). The thousands of microfluidic channels can be fabricated using one lithographic step. Therefore, this method generates very uniform fields even at regions close to the boundary, without recourse to any electrodes inside the channels.

5.5 Modeling of field nonuniformity

The residual nonuniformity of the field is characterized by the root-mean-square field distortion, defined as

$$\sqrt{\frac{\iint\limits_{\substack{array\\area}} \left|E - E_0\right|^2 dxdy}{\iint\limits_{\substack{array\\area}} \left|E_0\right|^2 dxdy}},$$

where E is the field to be evaluated, and E_0 is the ideal uniform field. The vertical field generated by a typical 24-electrode CHEF (Fig. 5.2B) has a RMS distortion of ~9%, according to computer simulation. Most distortions come from the regions near the electrodes. To evaluate the current injection method, let us assume that the electrical resistance of channels in parallel on each side of the array is $n\rho$, where ρ is the sheet resistance of the central area, and $n > 1$ (Fig. 5.3A). Computer simulation shows that the field is made uniform as the channel resistance becomes larger (Fig. 5.4A). In terms of the RMS field distortion, the current injection method outperforms the CHEF method

when $n > 2.1$. The distortion is largest at the four corners of the central area, in the case of vertical fields. The maximum angle of the field with respect to the vertical axis is shown in Fig. 5.4B. Note that the curve approaches $1/2n$ as n becomes larger. This is because at a corner, the horizontal component of the current density is $V/n\rho L$, where V is the electric potential at the corner, and L is the dimension of the central area (Fig. 5.4C). Similarly, the vertical component of the current density is $\sim 2V/\rho L$. The angle of the field at the corner with respect to the vertical axis is the ratio of the two components, which is $\sim 1/2n$. We see that the field is made uniform at the expense of its strength, for a given set of applied voltages. This is not a serious problem because microfluidic chips are generally small.

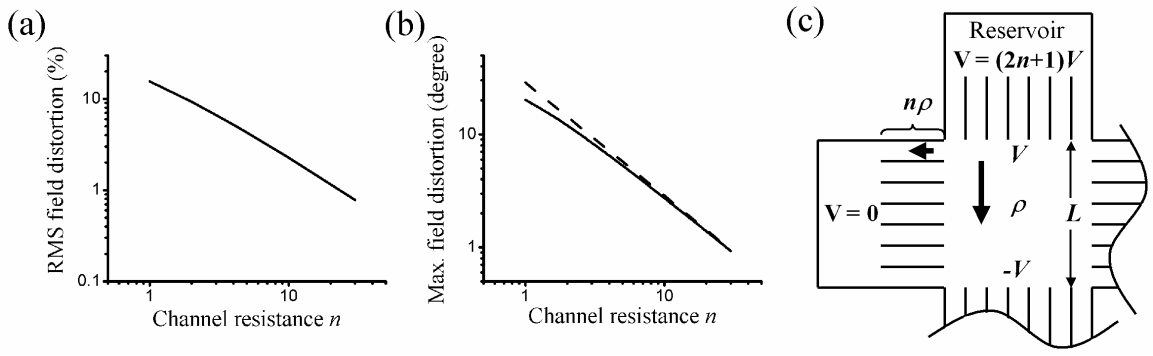

Fig. 5.4 (A) Computer calculated RMS field distortion as a function of channel resistance. (B) Maximum angle between the actual field and the perfectly homogeneous field. Dashed line: $1/2n$, estimated analytically. Solid line: computer simulated. (C) Microfluidic channels surrounding a square area.

5.6 Device design and fabrication

The DNA prism is a fully integrated analytical machine consisting of a hexagonally-packed array of micron-scale posts, sample injection and extraction channels, and structures for shaping uniform electric fields (Fig. 5.5) [10]. Our goal was to inject DNA into the post array using electric pulses, separate DNA fragments as they flowed through the array using alternating fields of different directions and strengths, and finally to collect the sorted DNA in microfluidic channels for further downstream analysis. Microfluidic channels surround the array and connect it to fluid reservoirs, where voltages are applied. The channels replace the many electrodes conventionally used to create uniform electric fields, as well as providing sample loading and collection ports [13]. Eight instead of four buffer reservoirs are used to reduce the resistance needed for a given uniformity goal. The resistance of each bundle of channels in parallel is designed to be 2.2 times as large as the sheet resistance of the array (n = 2.2). Computer simulation shows that the field distortion is about 1% around the center section of the array, where DNA is injected and fractionated.

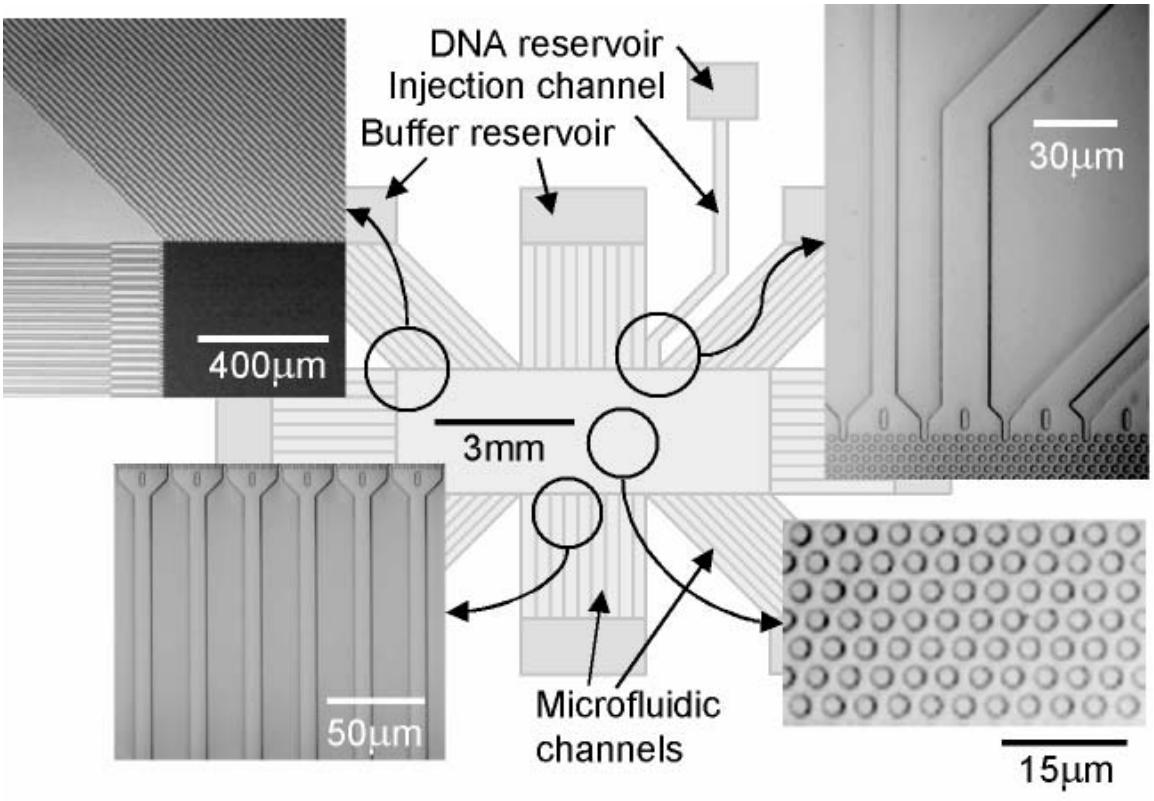

Fig. 5.5. Structure of the device illustrating the microfabricated sieving matrix integrated with the microfluidic channels. The post array is 3 mm x 9 mm, and the posts are 2 μm in diameter, 2 μm apart, and 2 μm tall. A single channel connecting to the DNA reservoir injects DNA through a 25 μm opening. The many microfluidic channels connecting to buffer reservoirs produce uniform electric fields over the sieving matrix by acting as electric current injectors [13].

The fabrication process includes only one lithographic step, which defines the posts and the channels. The pattern is transferred anisotopically to fuse silica with reactive ion etching (RIE), using CF_4 and H_2. The etch depth is up to 6 μm. Access holes contacting the external reservoirs were mechanically drilled. Finally, the substrate is tightly bonded to a piece of glass cover slip coated with RTV silicone to form enclosed fluidic channels.

5.7 Experimental results of uniform fields

We generated fields at 0^o, 60^o, and 90^o with respect to the horizontal axis in the DNA prism (Fig. 5.6). DNA molecules were stained with fluorescent dye, and observed with an optical microscope. First, a 60^o field of 31V/cm was applied. The DNA molecules formed a straight band as they traveled against the electric field (DNA is negatively charged), with the maximum deviation from the desired angle of ~2^o. We then switched the field to horizontal (Fig. 5.6B). The band moved at a constant speed in the horizontal direction. The trajectories of the molecules revealed that the field is now strictly horizontal. The band of the DNA is also very straight when the field is switched to vertical (Fig. 5.6C). We conclude that the device generates uniform fields over a large area at multiple angles.

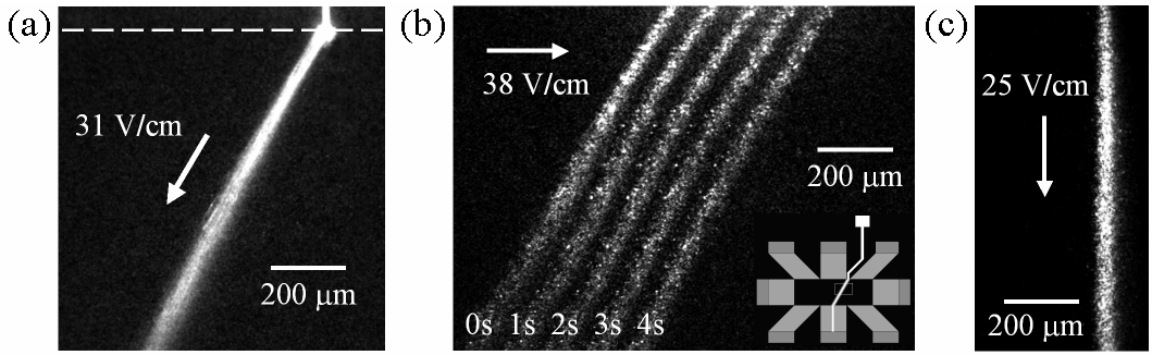

Fig. 5.6. Visualization of the field by fluorescence microscopy. (A) DNA injection at 60^o. The dashed line marks the boundary of the array. The arrow shows the direction of motion of DNA, which is opposite the field direction. (B) Overlay of time sequential fluorescent images of motion of DNA, to show spatial uniformity of electric field through steady motion of band. Band on left (0 s) is after DNA injection using electric field of -30^o with respect to vertical (52 V/cm), other four bands are at one second intervals with field of 38 V/cm in horizontal direction. (C) DNA injection at 90^o.

5.8 Application to genomic DNA separation

The device was used to separate bacterial artificial chromosomes (BAC), a class of recombinant DNA that plays a key role in genome projects [14]. 61 kb and 158 kb of BAC (18μm and 54μm long, respectively) were mixed and injected into the array by a vertical field (Fig. 5.7 top). The field was then switched alternatively between $+60^{o}$ and -60^{o} with respect to the horizontal axis to separate DNA (Fig. 5.7 middle). The DNA migrated towards the average field direction. Because long DNA molecules tangled around the posts more than short molecules did, they moved at a lower speed (3). The 61 kb DNA was separated from the 158 kb molecules in less than 7 seconds, well over three orders of magnitude faster than the conventional method [2–6].

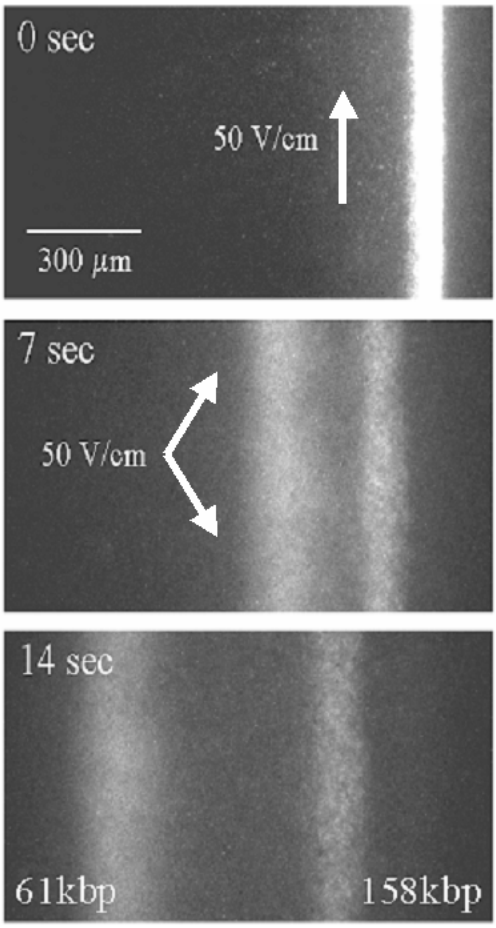

Fig. 5.7. Progress of separation of DNA mixture in microfabricated device, with loading by 50 V/cm vertical field (0 s), followed by separation after 7 s and 14 s with symmetric pulsing of 50 V/cm fields (± 60^{o} with respect to horizontal, 167 ms pulse duration). Small DNA fragments (61 kb) move faster than large ones (158 kb). Such a separation requires uniform fields to keep the bands straight and parallel. DNA is viewed by fluorescent microscopy.

5.9 Summary

A new method for generating tunable uniform electric fields over entire microfluidic arrays has been demonstrated. The current sources can easily be microfabricated with single lithographic process. Since no electrodes are needed in the microfluidic channels, bubble generation and electrode erosion problems do not exist.

The small number of voltage contacts makes the method practical for implementation, and the large number of resistors gives very uniform electric fields. The channels may be used to deliver and extract the DNA to and from the array. The current injection method is compatible with many functions of lab-on-a-chip devices, and should be useful for many practical microfluidic applications.

References

1. Sambrook, J.; Fritsch, E. F.; Maniatis, T. *Molecular Cloning: A Laboratory Manual, second edition*. (Cold Spring Harbor Laboratory Press, Cold Spring Harbor, NY).
2. Carle, G. F., Frank M. & Olson, M. V. *Electrophoretic separations of large DNA molecules by periodic inversion of the electric field. Science* **232**, 65-68 (1986).
3. Schwartz, D. C. & Cantor, C. R. *Separation of yeast chromosome-sized DNAs by pulsed field gradient gel electrophoresis. Cell* **37**, 67-75 (1984).
4. Chu, G., Vollrath, D. & Davis, R. W. *Separation of large DNA molecules by contour-clamped homogeneous electric fields. Science* **234**, 1582-1585 (1986).
5. Cox, E. C., Vocke, C. D. & Walter S. *Electrophoretic karyotype for Dictyostelium discoideum. Proc. Natl. Acad. Sci. U.S.A.* **87** (21), 8247-8251 (1990).
6. Sambrook, J., Fritsch, E. F. & Maniatis, T. *Molecular Cloning: A Laboratory Manual, second edition*. (Cold Spring Harbor Laboratory Press, Cold Spring Harbor, NY).
7. Volkmuth, W. D. & Austin, R. H. *DNA electrophoresis in microlithographic arrays. Nature* **358**, 600-602 (1992).
8. Bakajin, O. *et. al., Separation of 100 kilobase DNA molecules in 10 seconds. Anal. Chem.* **73**, 6053-6056 (2001).
9. T. A. J. Duke, R. H. Austin, E. C. Cox, and S. S. Chan, *Pulsed-field electrophoresis in microlithographic arrays, Electrophoresis* **17**, 1075-1079 (1996).
10. Huang, L. R.; Tegenfeldt, J. O.; Kraeft, J. J.; Sturm, J. C.; Austin, R. H.; Cox, E. C. *Nat. Biotechnol.* **2002**, *20(10)*, 1048–1051.
11. G. Chu, D. Vollrath, and R. W. Davis, *Separation of large DNA molecules by contour-camped homogeneous eectric felds, Science* **234**, 1582-1585 (1986).
12. J. Mathews, R. L. Walker, *Mathematical Methods of Physics, Second Edition.* (Addison-Wesley, 1970).
13. Huang, L. R. et. al. *Generation of large-area tunable uniform electric fields in microfluidic arrays for rapid DNA separation. International Electron Devices Meeting Technical Digest*, 363-366 (2001).
14. Osoegawa K. *et al*. *Bacterial artificial chromosome libraries for mouse sequencing and functional analysis. Genome Research* **10**, 116-128 (2000).

Chapter 6

DNA Prism II: High Speed Continuous Fractionation of Large DNA Molecules

6.1 Alternative methods for DNA separation

The analysis and fractionation of large DNA molecules plays a key role in many genome projects. The standard method, pulsed-field gel electrophoresis, is slow, with running times ranging from 10 to more than 200 hrs [1–5]. Alternative methods for sizing large DNA fragments have been developed in many laboratories. One approach, based on flow cytometry, measures fluorescence intensity as individual DNA molecules pass through a focused laser beam. DNA fragments up to ~200 kb have been sized in ~3 min by this method [6]. The DNA fragments can then be transported to different reservoirs according to size [7]. Another single-molecule sizing approach is to fully stretch DNA fragments and measure their contour lengths [8]. Alternatively, capillary gel electrophoresis using pulsed fields has been shown to separate mega-base DNA molecules in ~10 min [9].

Many microfluidic devices [10–24] for DNA separation have also been developed using microfabrication [25, 26]. These devices incorporate different physical principles

to separate DNA. In previous chapters, I have described the Brownian ratchet array and tango array, which can be used for DNA separation. Other designs include the entropic trap array, which consists of a series of many narrow constrictions (< 100 nm) separated by wider and deeper regions (a few microns), and which reduces the separation time to about 30 minutes [15]. Because the constrictions are fabricated to be narrower than the radius of gyration of large DNA molecules, they act as entropic barriers. The probability of a molecule overcoming the entropic barrier is dependent on molecular weight, and thus DNA molecules migrate in the entropic trap array with different mobilities. Larger molecules, with more degrees of configurational freedom, migrate faster in these devices.

6.2 Major advances presented by DNA prism

The DNA prism is evolved from a different microfluidic design—the hexagonal array of microposts [16, 17]. The early version of hexagonal array has been shown to separate DNA molecules in the 100 kb range in a few seconds; however, this device was limited in the amount of material that could be analyzed due to the shallowness of its sieving matrix, and the electrodes caused severe distortion of the electric field, which further limited the usefulness of this design.

The DNA prism presents three major advances over the microfabricated designs reviewed above. First, continuous-flow operation removes the limitation of the amount of sample the device can analyze. Second, the current injection method (previous chapter) has been integrated to generate and maintain uniform electric fields and very

precise sample injection [27]. And third, the speed and resolution, as well as the robustness of the DNA prism has been demonstrated using bacterial artificial chromosomes (BAC) and P1-derived artificial chromosome (PAC) inserts isolated by a standard miniprep protocol [28]. 61 kb to 209 kb DNA molecules were separated in 15 seconds, with ~13% resolution [29]. Further, because the array of micron-scale posts replaces the conventional cross-linked or entangled gel as the sieving media, and because high fields (~200 V/cm) are used, DNA molecules can be separated at speeds orders of magnitude faster than conventional techniques. Further, since the post arrays are just a few μm deep, the total volume of buffer inside the device is of order 100 nL, and heat is rapidly dissipated. Consequently cooling of the device is not required. By comparison, conventional pulsed field gel devices typically contain liter quantities of electrophoresis buffer which is continuously circulated through a cooling chamber.

6.3 Fractionation of bacterial artificial chromosomes

We sorted BAC and PAC inserts of 61 kb, 114 kb, 158 kb and 209 kb (Fig. 1, 2). BAC's and PAC's were isolated from *E. coli* stains RPCI 21 168-F5, RPCI 21 539-K14, RPCI 22 49-E10, and RPCI 23 200-J16 by standard methods [28]. Plasmid preparations were digested with *Not*I and the digestion buffer exchanged with 1/2x TBE using centrifugal filters (Microcon YM-100 from Amicon). The electrophoresis buffer was 0.5X TBE containing 0.1% POP-6, a performance optimized linear polyacrylamide (Perkin-Elmer Biosystems) and 10 mM dithiothreitol (DTT) added to suppress electroosmotic flow and photo-bleaching, respectively. DNA was stained with TOTO-1

(Molecular Probes) at a ratio of 1 dye molecule per 10 base pairs. The starting DNA concentration was about 10 ng/μL. Images were recorded by epi-fluorescence microscopy. Excitation was at 488 nm, and fluorescence was observed using low-pass filter (495 nm). A Roper intensified CCD camera was used for image capture. DNA preparations used in this study were also characterized by pulsed field gel electrophoresis as previously described.

A wide range of pulsing conditions was tested, including field strengths from ~20 V/cm to ~250 V/cm, and square pulse durations from 10 msec to 500 msec. Separation occurred under pulse conditions of low field strength in combination with long pulse duration, or higher field strengths with short pulse durations (Fig. 1). By observing the molecular size in each separation stream at high-magnification, we found that small molecules move close to the average field direction, while large molecules migrate towards the strong pulse direction, as expected. Further, the migration direction and band sharpness depends on the exact pulse conditions. While low strength pulses (~50 V/cm) combined with long duration typically separate the four species into only two bands (Fig. 1A), higher field strengths (~200 V/cm) combined with shorter duration (~50 msec) resolve all four species (Fig. 1B). The separated molecules are collected in different channels at the edge of the device (Fig. 1C). Under high fields (~200 V/cm), the separation time over 3 mm is 15 sec.

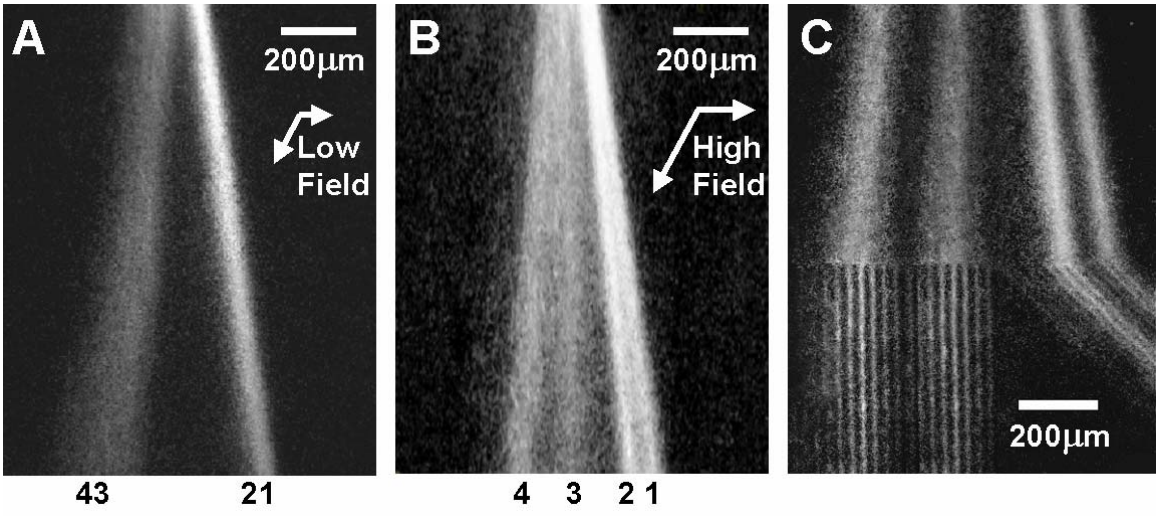

Figure 1 Fluorescence micrographs of continuous DNA separation under different field strengths. Long and short arrows point to the DNA migration directions during strong and weak pulses, respectively. Band assignment for the BAC and PAC inserts: (1) 61 kb, (2) 114 kb, (3) 158 kb, (4) 209 kb. (A) Four species are separated into only two bands using 250 msec square pulses of 32 V/cm and 20 V/cm alternating at 2 Hz. (B) All four species are resolved using 40 msec square pulses of 240 V/cm and 150 V/cm alternating at 12.5 Hz. (C) Separated molecules are collected in different channels, and routed to different reservoirs.

The migration angle of DNA molecules is a function of the pulse duration (Fig. 2A). Using 55 msec square pulses of 240 V/cm and 150 V/cm, the four species of DNA are separated into three bands (Fig. 2A, 55ms). The brighter of the three contains 61 kb and 114 kb molecules. However, as we decreased the duration to 40 msec (Fig. 2A, 40ms), the large molecular weight bands (158 kb and 209 kb) shifted towards the average field direction, while the originally unresolved band of small molecules (61 kb and 114 kb) split into two. All four species were then resolved. Although the bands shift with pulse duration in ways not yet fully understood, the changes are very reproducible. The fact that the separation depends on pulse duration is not surprising—it exists for standard pulsed-field gel electrophoresis (PFGE) as well. In fact, PFGE uses different pulse durations (typically from 0.1 sec to 40 sec) to resolve different molecular-weight ranges.

Although the continuous-flow prism requires a fixed pulsing duration to operate at steady-state, different durations can be used in consecutive runs, each of which analyzes a different molecular-weight range chosen to optimize resolution.

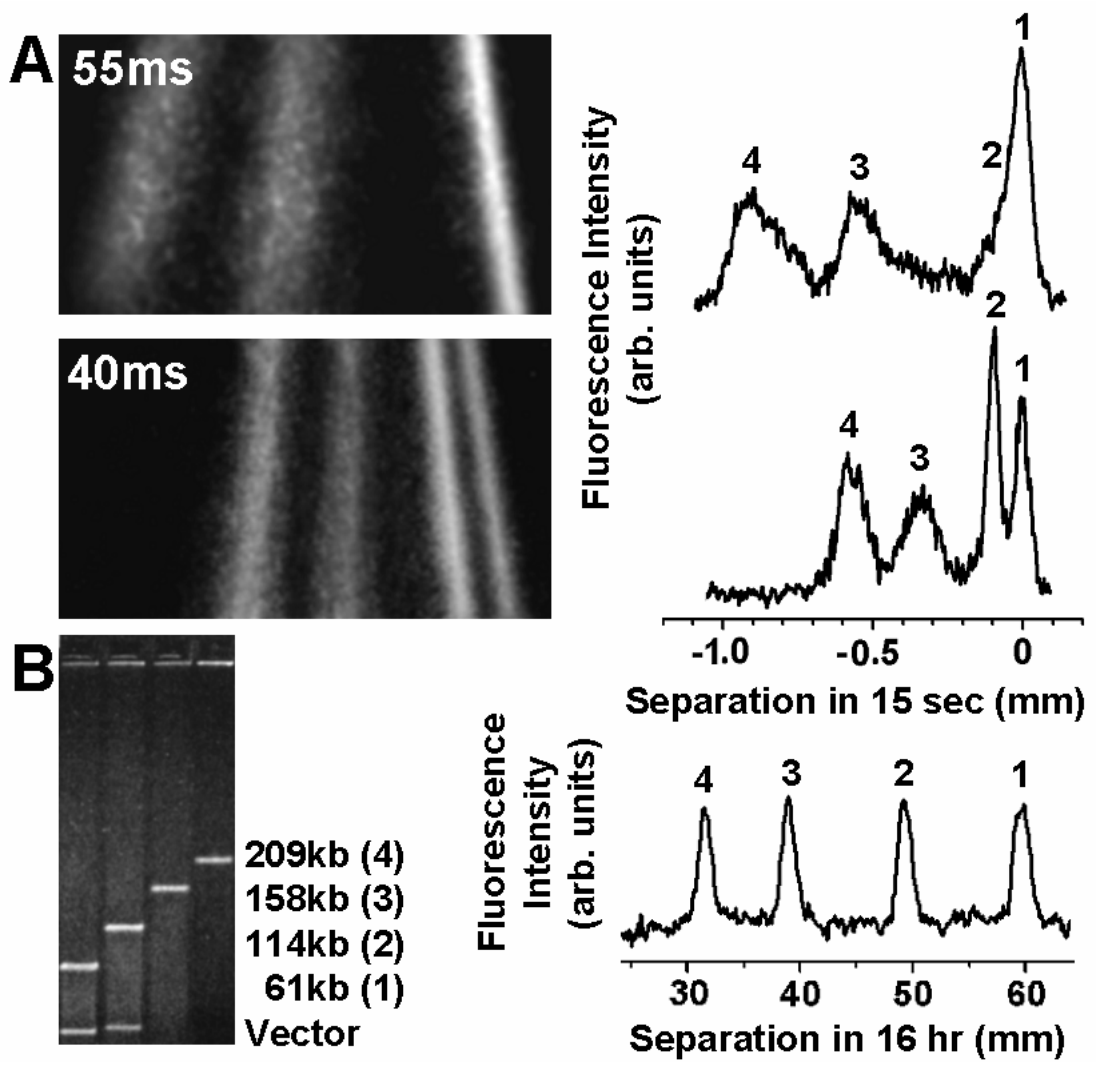

Figure 2 Separation of BAC and PAC inserts at different frequencies. (A) Separation in 15 seconds using the DNA prism. Fluorescence micrographs show the separated DNA bands from 2.5 to 3 mm below the injection point. The fluorescence intensity profiles are scanned at 3 mm from the injection point, with the origin of the horizontal axis defined as the average field direction. Peak assignment: (1) 61 kb, (2) 114 kb, (3) 158 kb, (4) 209 kb. The resolution in the 114 kb to 209 kb range is 11% to 15% at 55 msec, and 16% to 19% at 40 msec. The separation time using a 3 mm long sieving matrix is ~15 sec. (B) Separation in 16 hours using conventional pulsed field gel electrophoresis. Pulsing conditions: 6 V/cm pulses 120^{o} apart, duration linearly ramped from 0.1 sec to 40 sec in 16 hours [28]. The resolution using this protocol is ~7%. The horizontal axis of the fluorescence intensity profile is defined as the DNA migration distance from the loading wells. Peaks for the vectors not shown.

6.4 Comparison with conventional methods

The resolution is about 11% to 15% in the 100 kb to 200 kb range (Fig. 2A, 55 msec) [29]. Although band broadening in the DNA prism is not yet fully understood, it seems likely that the degree to which all molecules are fully stretched and therefore back–track accurately currently limits resolution. Because high fields stretch DNA molecules more than low fields, and short pulse durations reduce the time for relaxation, molecules under these conditions elongate more fully and back track accurately (Fig. 1). The post size and spacing of the array should also affect the stretching of DNA, particularly of small molecules. The 61 kb and 114 kb inserts are poorly resolved (Fig. 2A) because they are too small to interact with the posts and be fully stretched. In fact, 61 kb molecules never deviate from the average field direction, suggesting that these molecules do not elongate and back track. This result is supported by other experiments and theoretical calculations [30, 31], which show that randomly-coiled DNA molecules shorter than ~100 kb are smaller than the constrictions in the array (2 μm posts and 2 μm spacings), and thus little stretching should occur. Although the resolution is not yet as sharp as can be achieved by highly-optimized conventional methods (Fig. 2B, running time = 16 hours, resolution ~ 7%), it is clear that the resolution improves with separation distance, and with pulse tuning, neither one of which has yet been fully optimized (Fig. 1 and 2A). In this regard, we point out that the resolution of the four inserts shown in Fig. 2B required a linear duration ramp from 0.1 to 40 sec over 16 hrs. At constant pulse duration, conditions similar to those used with the DNA prism (Fig. 2A, 40 msec) these four species would not separate or separate very poorly.

Because of the small scale of the microfluidic devices and the extremely low Reynolds number (on the order of 10^{-3}), there is no turbulence in this device [32]. Consequently, large DNA molecules do not break as they move through them. The lack of shearing is evident from the fact that resolution increases with field strengths (Fig. 1). If high electric fields had broken the DNA, then clearly band width would be wider at the higher field. This is contrary to our observation (Fig. 1 and 2).

In conventional gel electrophoresis [1–5], run-to-run reproducibility is mainly influenced by the gel matrix concentration, the buffer strength, and temperature. The DNA prism devices showed good run-to-run reproducibility: no change in separation angles were observed when the device was operated overnight, and the separation angles were always the same for a given set of pulsing conditions, regardless of the conditions applied during sample loading. This is because the microfabricated post array replacing the conventional gel matrix has accurate pore sizes, while the thin array generates very little heat. Further, although we used small buffer reservoirs (typically ~20 μL per reservoir), the amount of buffer inside the device is only ~100 nL, and therefore the buffer strength remains constant over a long time. When the small reservoirs are sealed with Scotch tape, no buffer evaporation or gas generation can be observed over 10 hours of operation. The device-to-device reproducibility is also good—the variations in the post and channel dimensions are typically less than 5%, using standard semiconductor processing techniques. We tested four devices and observed similar separation patterns, using running buffer and DNA samples freshly made and stained.

6.5 Throughput of DNA prism

The current version of the DNA prism has a throughput of ~10^4 molecules/sec (~10 ng/hour or ~1 μL/hour). This rate is high compared to other unconventional techniques, and certainly high enough for efficient sequencing library preparation. Sample recovery from the device is currently limited by the ability to pipette small volumes of liquid; however we believe this problem is offset by our ability to direct fractionated DNA into collection channels (Fig. 1C), where samples can be routed on-chip to other compartments for further analysis. By comparison, the entropic trap array [15] and our previous work on hexagonal post arrays [16, 17] are limited in throughput (~10 pg/hour) because of the small sample plug. Other continuous-flow techniques also have lower throughput—the asymmetric obstacle arrays [12, 13] typically ~100 pg/hour because of the low flow speed required for diffusion-based, and fluorescence-activated cell sorting methods typically process ~100 molecules per second (~100 pg/hour).

6.8 Summary

In summary, the DNA prism technique has substantial advantages over other devices reported in the literature to separate high molecular weight DNA. First, the DNA prism sorts each molecule at high speeds, with running times of typically ~15 sec. This is more than 1000 times faster than the conventional pulsed field gel electrophoresis (10-240 hours). Compared to other novel methods, the prism is 9 times faster than flow cytometry (15 sec *vs.* 130 sec [6]), 40 times faster than pulsed field capillary

electrophoresis [9] (~10 min), and over 100 times faster than the entropic trap arrays [15] (~30 min) and the asymmetric obstacle arrays [12, 13] (~2 hours). Further, the prism device has better resolution (~13 %) than the entropic trap arrays, the asymmetric obstacle arrays, and an earlier version of the hexagonal post arrays, which demonstrated resolution of 50% to 100% in the 100 kb to 200 kb range.

References

1. Carle, G. F., Frank M. & Olson, M. V. Electrophoretic separations of large DNA molecules by periodic inversion of the electric field. *Science* **232**, 65-68 (1986).
2. Schwartz, D. C. & Cantor, C. R. Separation of yeast chromosome-sized DNAs by pulsed field gradient gel electrophoresis. *Cell* **37**, 67-75 (1984).
3. Chu, G., Vollrath, D. & Davis, R. W. Separation of large DNA molecules by contour-clamped homogeneous electric fields. *Science* **234**, 1582-1585 (1986).
4. Cox, E. C., Vocke, C. D. & Walter S. Electrophoretic karyotype for *Dictyostelium discoideum*. *Proc. Natl. Acad. Sci. U.S.A.* **87** (21), 8247-8251 (1990).
5. Sambrook, J., Fritsch, E. F. & Maniatis, T. *Molecular Cloning: A Laboratory Manual, second edition*. (Cold Spring Harbor Laboratory Press, Cold Spring Harbor, NY)
6. Huang, Z. *et. al.* Large DNA fragments sizing by flow cytometry: application to the characterization of P1 artificial chromosome (PAC) Clones. *Nucleic Acids Res.* **24**, 4202-4209 (1996).
7. Chou, H. P., Spence, C., Scherer, A. & Quake, S. R. A microfabricated device for sizing and sorting DNA. *Proc. Natl. Acad. Sci. USA* **96**, 11-13 (1999).
8. Guo, X., Huff, E. J. & Schwartz, D. C. Sizing single DNA molecules. *Science* **359**, 783-784 (1992).
9. Kim, Y. & Morris, M. D. Rapid pulsed field capillary electrophoretic separation of megabase nucleic acids. *Anal. Chem.* **67**, 784-786 (1995).
10. Volkmuth, W. D. & Austin, R. H. DNA electrophoresis in microlithographic arrays. *Nature* **358**, 600-602 (1992).
11. Chou, C. F. *et. al.* Sorting by diffusion: an asymmetric obstacle course for continuous molecular separation. *Proc. Natl. Acad. Sci. USA* **96,** 13762-13767 (1999).
12. Cabodi, M., Chen, Y. & Craighead, H. Continuous separation of biomolecules by the laterally asymmetric diffusion array with out-of-plane sample injection. *Electrophoresis* **23**, 3496 (2002).
13. Huang, L. R.; Silberzan, P; Tegenfeldt, J. O.; Cox, E. C.; Sturm, J. C.; Austin, R. H.; Craighead H. *Phys. Rev. Lett.* **2002**, *89*, 178301–178304.
14. A. Oudenaarden and S. G. Boxer, Brownian Ratchets: Molecular Separations in Lipid Bilayers Supported on Patterned Arrays, *Science* **285**, 1046 (1999).
15. Han, J. & Craighead, H. G. Separation of long DNA molecules in the microfabricated entropic trap array. *Science* **288**, 1026-1029 (2000).
16. Bakajin, O. *et. al.* Separation of 100 kilobase DNA molecules in 10 seconds. *Anal. Chem.* **73**, 6053-6056 (2001).
17. T. A. J. Duke, R. H. Austin, E. C. Cox, and S. S. Chan, *Pulsed-field electrophoresis in microlithographic arrays, Electrophoresis* **17**, 1075-1079 (1996).
18. Huang, L. R.; Tegenfeldt, J. O.; Kraeft, J. J.; Sturm, J. C.; Austin, R. H.; Cox, E. C. *Nat. Biotechnol.* **2002**, *20(10)*, 1048–1051.
19. M. Schena, D. Shalon, R. W. Davis, and P. O. Brown, *"Quantitative Monitoring of Gene Expression Patterns with a Complementary DNA Microarray," Science* **270**, 467 (1995).

20. M. A. Burns, B. N. Johnson, S. N. Brahmasandra, K. Handique, J. R. Webster, M. Krishnan, T. S. Sammarco, P. M. Man, D. Jones, D. Heldsinger, C. H. Mastrangelo, and D. T. Burke, *"An Integrated Nanoliter DNA Analysis Device," Science* **282**, 484 (1998).
21. M. U. Kopp, A. J. de Mello, and A. Manz, *"Chemical Amplification: Continuous-Flow PCR on a Chip," Science* **280**, 1046 (1998).
22. A. Hatch, A. E. Kamholz, K. R. Hawkins, M. S. Munson, E. A. Schilling, B. H. Weigl, P. Yager, *"A rapid diffusion immunoassay in a T-sensor," Nature Biotechnology* 19, 461 (2001).
23. T. Thorsen, S. J. Maerkl, and S. R. Quake, *"Microfluidic Large-Scale Integration," Science* **298**, 580 (2002).
24. D. L. Huber, R. P. Manginell, M. A. Samara, B. Kim, and B. C. Bunker, *"Programmed Adsorption and Release of Proteins in a Microfluidic Device," Science* **301**, 352 (2003).
25. E. W. Becker *et. al*., Microelectronic Engineering 4 (1986), pages 35 to 56.
26. H. Becker *et. al*., J. Micromech. Microeng. 8 (1998), pages 24 to 28.
27. Huang, L. R. et. al. Generation of large-area tunable uniform electric fields in microfluidic arrays for rapid DNA separation. *International Electron Devices Meeting Technical Digest*, 363-366 (2001).
28. Osoegawa K. *et al*. Bacterial artificial chromosome libraries for mouse sequencing and functional analysis. *Genome Research* **10**, 116-128 (2000).
29. Giddings, J. C. *Unified Separation Science* (John Wiley & Sons, New York, 1991).
30. Doi, M. & Edwards, S. F. *The Theory of Polymer Dynamics* (Oxford U. P., Oxford, England, 1989).
31. Smith, S. B., Finzi, L. & Bustamante, C. Direct mechanical measurements of the elasticity of single DNA molecules by using magnetic beads. *Science* **258**, 1122-1126 (1992).
32. Feynman, R. P., Leighton, R. B. & Sands, M. *The Feynman Lectures on Physics Vol.2*. (Addison-Wesley Publishing Co., Inc., Reading, MA) p.41-5.

Chapter 7

DNA Prism III: Physical Principles for Optimization

7.1 Introduction

In the previous chapter, we demonstrated continuous sorting of large DNA molecules (61 kilo-base pair to 209 kb) according to size in 15 seconds, using the DNA prism device [1]. However, the device's separation characteristics are complicated and poorly understood. The goal of this chapter is to understand and optimize these characteristics [2].

7.2 Constant fraction elongation model

When electric pulses are applied to the sieving array, DNA molecules migrate at different directions according to their molecular weights (Fig. 7.1) [3, 4]. The electric pulses are applied alternatively at two directions 120° apart, with stronger intensity along the first direction than the second. When the first electric pulse is applied, molecules of all sizes migrate similar distances because the DNA mobility is independent of the molecular weight (Fig. 7.1.a.i and 7.1.a.ii). As the field direction is rotated by 120° and its intensity weakened, molecules backtrack through channels formed by the post array

(Fig. 7.1.a.iii). The net motion of a molecule during a cycle is size-dependent. Mathematically, a molecule of length L^* in the array migrates $d_1 - L^*$ and $d_2 - L^*$ during the first and second pulse respectively (Fig. 7.1.a.iii), where d_1 and d_2 are the migration distances of small molecules that do not backtrack. Therefore, the net motion $\boldsymbol{N}$ in a cycle is the vector sum of the two distances,

$$\boldsymbol{N} = (d_1 - L^*)\,\mathbf{e}_1 + (d_2 - L^*)\,\mathbf{e}_2 \qquad (1)$$

where $\mathbf{e}_1$ and $\mathbf{e}_2$ are the unit vectors at the electric force directions. When $L^* < d_2 < d_1$, $\boldsymbol{N}$ points to different directions according to the molecular length L^*. While small molecules ($L^* << d_2$) migrate at the average electric force direction ($d_1\,\mathbf{e}_1 + d_2\,\mathbf{e}_2$), large molecules move more towards the strong pulse direction ($\mathbf{e}_1$). When $L^* > d_2$ (Fig. 7.1.b), molecules cannot reorient entirely, and move along $\mathbf{e}_1$.

If DNA molecules inside the sieving array are stretched to a constant fraction of their full lengths ($L^* = c\,L_0$, where $c \leq 1$ and L_0 is the full length), the migration angle with respect to the average force direction would be roughly a linear function of molecular weight (Fig. 7.2a). However, experiments showed "biphasic" separation characteristics under low fields (Fig. 7.2a and 7.2b): molecules smaller than a certain molecular weight threshold migrated towards one direction, and those larger than the threshold towards another direction [5]. This "constant fraction elongation model" fits experimental data poorly.

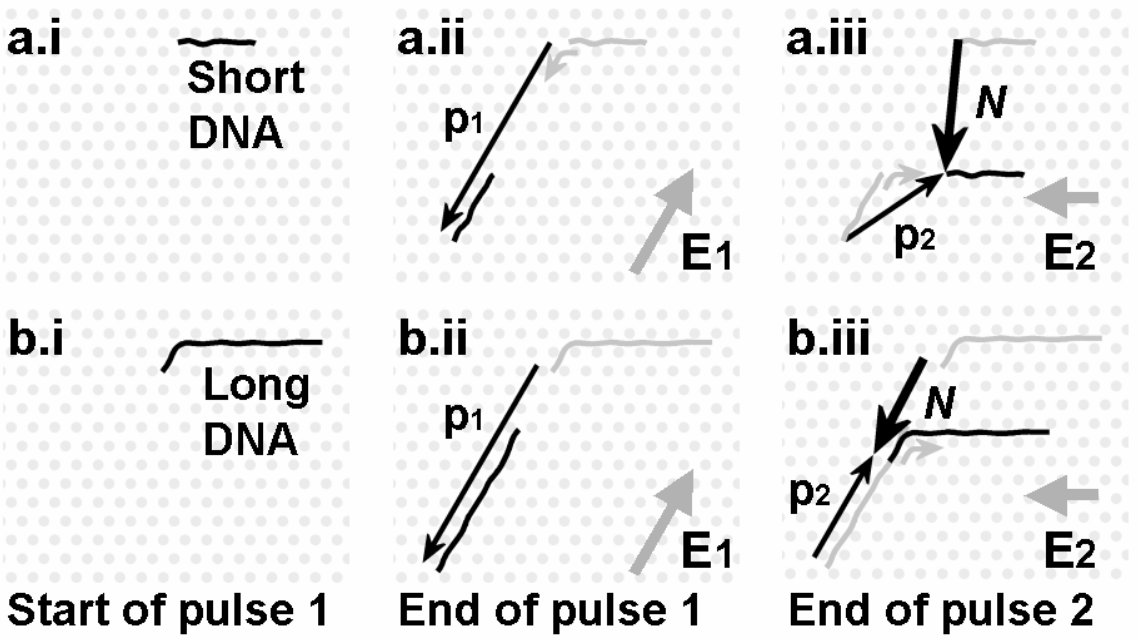

Fig. 7.1. Schematic contrasting motion of short (a.i, a.ii and a.iii) and long (b.i, b.ii and b.iii) DNA molecules over one cycle of electric pulses in the prism device, showing size dependent direction of motion. (a.i, b.i) Starting position of molecule at beginning of pulse. (a.ii, b.ii) Position at end of first pulse with electric field E_1 and displacement p_1 during first pulse shown. (a.iii, b.iii) Position at end of second pulse with weaker electric field E_2 during second pulse. Molecules backtrack. Displacement during pulse is p_2 and net displacement in a cycle is ***N***. Note p_2 differs for long and short molecules because long molecules do not backtrack off posts. Net motion over full cycle ***N*** therefore depends on size.

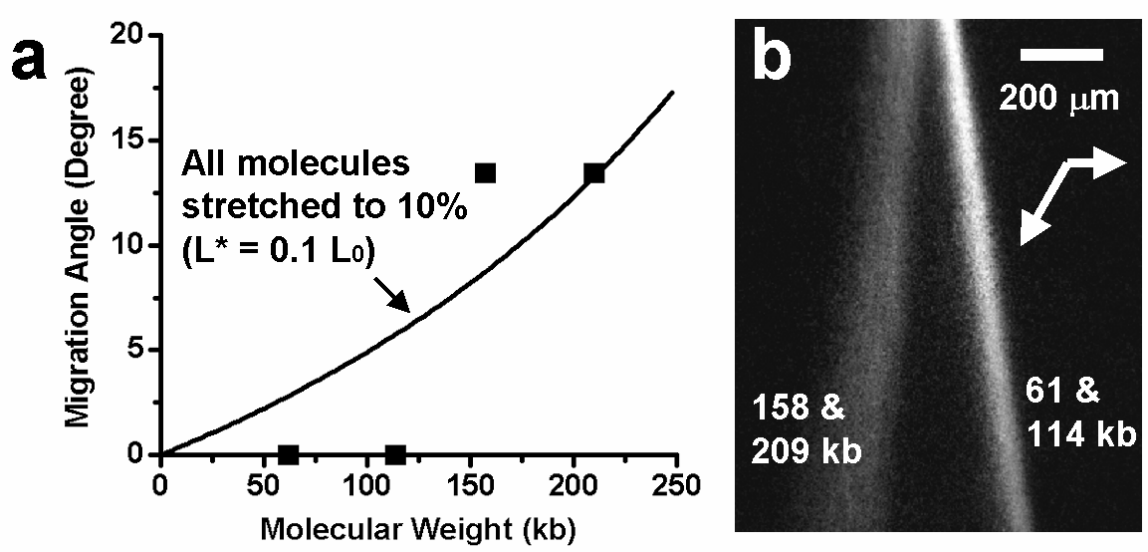

Fig. 7.2. "Biphasic" separation under low fields, poorly fitted by "constant fraction elongation model." (a) Migration angle dependence on molecular weight calculated by Eq. (1) assuming all molecules stretched to 10 % of their full lengths (solid curve). The squares are the data points measured from (b). (b) Fluorescent micrograph of four sizes of DNA molecules separated into two bands in the array by alternating 250 msec pulses of 32 V/cm and 20 V/cm. Arrows show directions of electric forces.

7.3 Damped spring model

The discrepancy between the model and the experiment arises from the fact that molecules of different molecular weights are stretched to different extents. Although DNA molecules are linear strands whose full contour lengths scale with their molecular weights, they are randomly coiled by thermal agitation under no external forces [6–8]. In fact, a DNA strand acts empirically like a spring—— the end-to-end distances L^* are nearly proportional to the force applied until it approaches the molecule's full length L_0 (Fig. 7.3a) [7]. We gain understanding of the prism device by building a model that incorporates this restoring force, the viscous drag, and the electric force. When a

molecule is moving in the post array under electric fields, it is going through cycles of elongation and relaxation (Fig. 7.3b). The stretching phase occurs at the beginning of each electric pulse, when the molecule hooks on the posts (Fig. 7.3b1). As soon as the molecule slides of the posts, it starts to relax (Fig. 7.3b2).

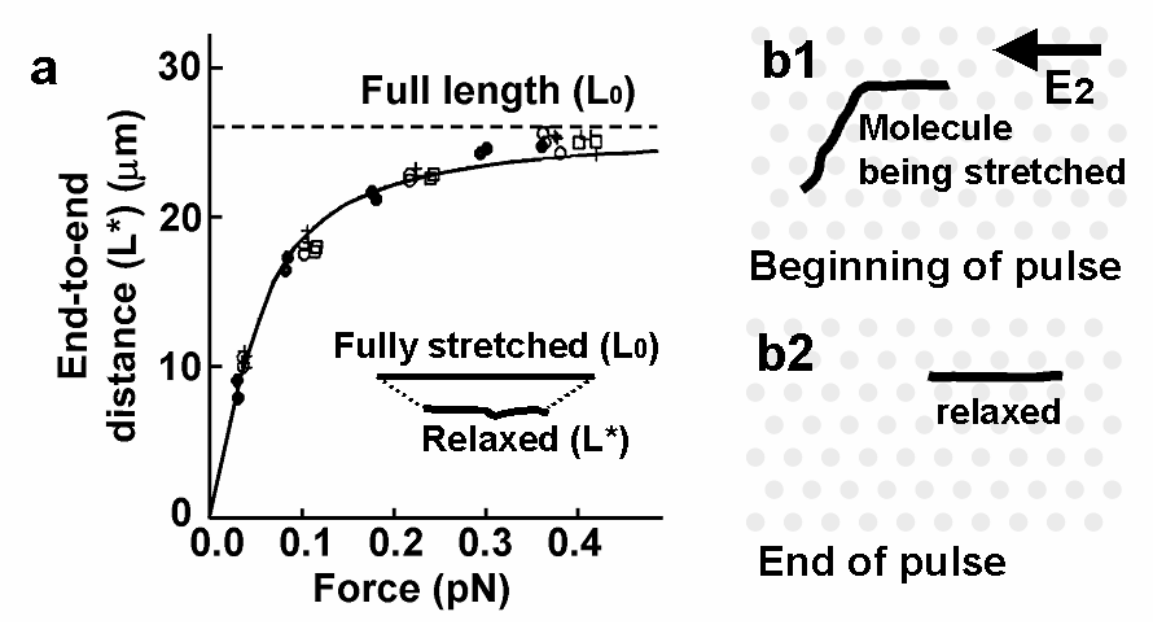

Fig. 7.3. (a) End-to-end distance of a 97 kb DNA molecule vs. stretching force [7]. (b1) A DNA strand in the array is being stretched at the beginning of each pulse, because each segment aligned with the field experiences stronger force than those at 60^{o} with respect to the field. (b2) The DNA molecules starts to coil once it reorients completely.

We assume that DNA molecules obey Hooke's law. This assumption holds if the fields are low and the molecules are stretched to under ~50% of their full lengths (Fig. 7.3a, $L^* < ½\ L_0$). A segment of a DNA strand can be mathematically specified as its contour distance z from one end of the molecule. The entire molecule's conformation

state is described by the positions x of every segment z. The equation of motion for a molecule in one dimension is therefore

$$\rho E - \frac{\rho}{\mu}\frac{\partial x}{\partial t}\frac{\partial x}{\partial z} + k\frac{\partial^2 x}{\partial z^2} = 0 \qquad (2)$$

where ρ is the linear charge density of DNA, μ is the mobility in free solution, and k is the spring constant of a unit-length strand. The first term of the equation represents the electric force, the second term the viscous drag, and the third term the restoring force. The inertial term is ignored because of the extreme small Reynolds' number [9]. Although the drag term is quadratic in x, rendering the equation unsolvable analytically, qualitative insights can be gained by assuming that $\frac{\partial x}{\partial z}$ is roughly a constant at all times. The linearized equation can be solved analytically by the technique of separation of variables.

The equation shows that the degree to which molecules are stretched depends on the molecular weight. For example, a tethered molecule will be stretched to $\frac{\rho E}{2k}L_0^2$, where L_0 is the full contour length of the molecule. The end-to-end distance scales with the square of molecular weight because the electric force scales with the molecular weight, while the spring constant are inversely proportional to it. Moreover, by solving the equation, we find that relaxation time constants (for different modes) of a molecule scale with L_0^2. Small molecules relax much faster than larger ones. This result is similar to experimental measurements found in the literature [8], which reports an exponent of 1.6.

From this simple consideration, we see that the end-to-end distance at the change of electric fields is

$$L^* = \alpha L_0^2 e^{-\frac{\beta}{L_0^2}t}, \quad (3)$$

where t is the pulse duration, and α and β are fitting parameters.

Equation (3) qualitatively explains the "biphasic" separation character under low fields (Fig. 7.4). According to the model, the biphasic behavior arises from the poor stretching and the rapid relaxation of small molecules. Further, molecules shorter than the center-to-center post spacing will not deviate from the average force direction, whereas those longer than the migration distance during the weak pulse (d_2) will co-migrate towards the same direction (Fig. 7.4a, b). The maximum migration angle in the model is the strong field direction. The measured angle is always smaller than the model predicted. Although the mechanism for this behavior is poorly understood, we speculate that it is due to the herniation of large molecules.

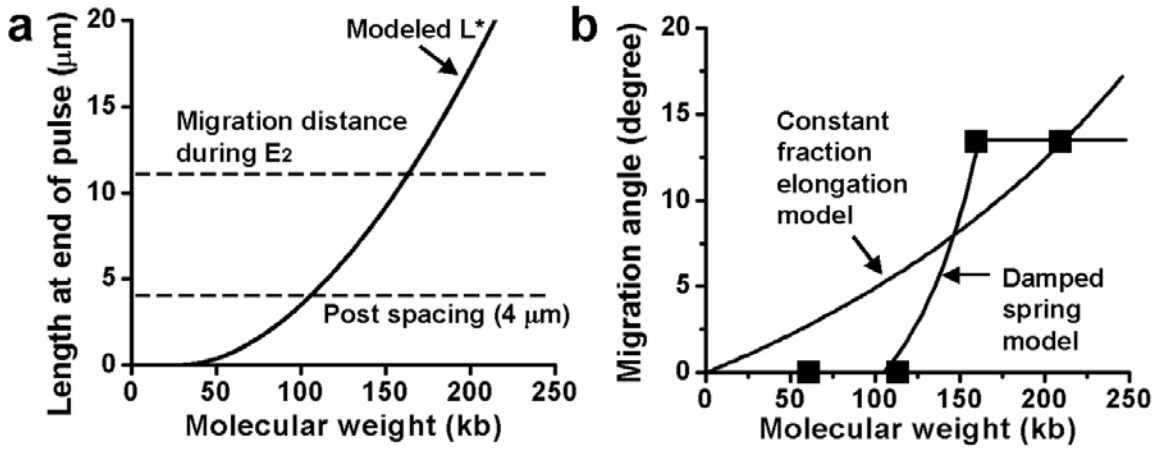

Fig. 7.4. (a) End-to-end distance of molecule calculated from Equation (3), with α = 0.004 m^{-2}, and βt = 320 m^2. (b) Migration angle (solid curve) calculated from the length modeled in (a) fits data (solid squares) for 250 msec pulses of 32 V/cm and 20 V/cm.

7.4 High field behavior

To achieve approximately linear separation, molecules should be highly stretched. Therefore high fields should be used to more fully stretch all molecules. Fig. 7.5 shows improved linearized performance achieved by increasing fields from 32 V/cm (Fig. 7.2) to 240 V/cm (Fig. 7.5).

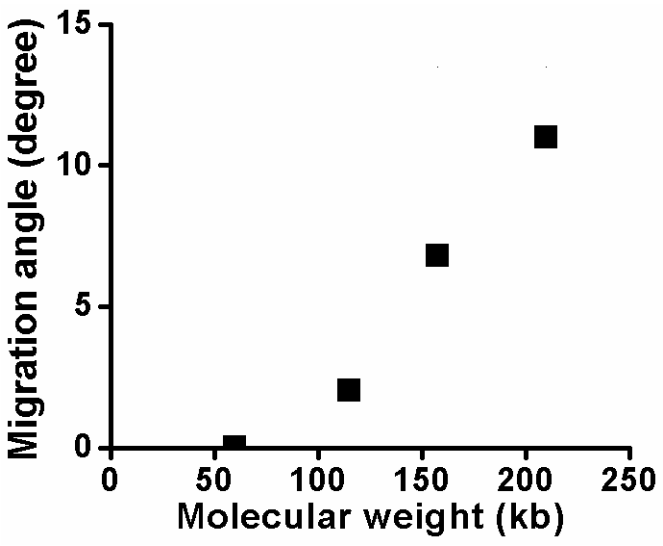

Fig. 7.5. Improved device characteristics under high fields and shorter pulses. The high-field conditions are 40 msec square pulses of 240 V/cm and 150 V/cm.

7.5 Summary

A model has been developed to qualitatively understand the behavior of the DNA prism device that continuously fractionates DNA in an array of microposts. The critical parameter is the degree of stretching of DNA, which depends on the electric field strengths and pulsing durations. While low fields result in biphasic separation behavior, high fields create more linear separation characteristics due to increased stretching. Future work includes quantitative understanding of the frequency dependence of stretching, and the effect of post size on DNA separation.

References

1. L. R. Huang *et al.* "A DNA prism for high-speed continuous fractionation of large DNA molecules," *Nat. Biotechnol.* **2002**, *20(10)*, 1048–1051.
2. L. R. Huang, *et. al, "A DNA Prism: Physical Principles for Optimizing a Microfabricated DNA Separation Device," International Electron Devices Meeting Technical Digest*, 211 (2002).
3. O. Bakajin, *et al.*, "Separation of 100 kilobase DNA molecules in 10 seconds," *Anal. Chem.* **73**, 6053-6056 (2001).
4. T. A. J. Duke, R. H. Austin, E. C. Cox, and S. S. Chan, *Pulsed-field electrophoresis in microlithographic arrays, Electrophoresis* **17**, 1075-1079 (1996).
5. Huang, L. R.; Tegenfeldt, J. O.; Kraeft, J. J.; Sturm, J. C.; Austin, R. H.; Cox, E. C. *Nat. Biotechnol.* **2002**, *20(10)*, 1048–1051.
6. Doi, M. & Edwards, S. F. *The Theory of Polymer Dynamics* (Oxford U. P., Oxford, England, 1989).
7. S. B. Smith, L. Finzi, and C. Bustamante, "Direct mechanical measurements of the elasticity of single DNA molecules by using magnetic beads," *Science* **258**, 1122-1126 (1992).
8. T. T. Perkins, S. R. Quake, D. E. Smith and S. Chu, "Relaxation of a single DNA molecule observed by optical microscopy," *Science* **264**, 822-826 (1994).
9. Feynman, R. P., Leighton, R. B. & Sands, M. *The Feynman Lectures on Physics Vol.2*. (Addison-Wesley Publishing Co., Inc., Reading, MA) p.41-5.

Chapter 8

Conclusion

8.1 Summary

We started our work studying microfabricated Brownian ratchet arrays for separation of biological molecules, specifically nucleic acids, according to diffusion coefficients. The separation process is based on molecular diffusion, a process which is intrinsically slow. We demonstrated that under stringent control of electric fields and precise delivery of sample molecules, the array can be used to sort DNA molecules in the ~100 kb range according to molecular weights. Further, we showed that the physical size of the molecules being separated played a critical role in the operation of the Brownian ratchet arrays. Previously, it was thought that small molecules could be separated with higher speeds because they diffuse faster. Our work shows that there exists a critical particle size threshold, which is related to the size of the narrowest feature through which the particles must pass in the array, and below which particles are incapable of being ratcheted. This points to the importance of very narrow gaps in the obstacle array if the separation of small particles is desired.

We developed a systematic method for optimizing the separation speed and resolution of Brownian ratchet arrays, where the key parameter was the direction of the

driving flow with respect to the array orientation. An order-of-magnitude improvement in the separation speed and resolution over the previous design of the Brownian ratchet array were demonstrated, using this flow tilting method.

Inspired by the flow tilting method, we invented a method for particle separation according to size, which does not rely on molecular diffusion. The resulting device, which we call the tango array, operates at astonishingly high speeds and resolutions. The method is based on two deterministic transport modes. High flow speed increased the resolving power by reducing the effect of Brownian motion, an effect now considered detrimental for the tango array, and one percent difference in particle size was routinely resolved in a running time of 40 s.

Although the tango arrays sorts beads with great speed and resolution, it failed to separate floppy molecules, such as DNA in the ~100 kb range, with similar speed and resolution. We developed a new class of devices, named DNA prisms, for high-speed DNA separation. The work on DNA prisms is a continuation of our attempt to perform pulsed-field electrophoresis with microfabricated arrays of posts replacing the conventional gel matrices. Because of the small scale of such microfabricated structures, sample loading, visualization, and field uniformity and tenability became serious problems that hampered the progress of our early attempts. We cracked these problems by using microfluidic channels surrounding the post array for accurate sample loading and the generation of tunable uniform fields. We further developed a new pulsing scheme consisting of asymmetric fields alternating in two directions, which removed the

limit of the amount of sample the device can analyze. The DNA prism device was tested with bacterial artificial chromosomes, to show that the microfabricated device is compatible with real biological samples. Three orders of magnitude improvement in separation speed over the conventional pulsed-field gel electrophoresis was demonstrated using the DNA prism.

A physical model for explaining the complex separation behavior of DNA prism devices was developed. This model shows that the biphasic separation behavior is due to uneven stretching of DNA molecules during separation. Uniform stretching of molecules to their full lengths can be achieved under high field conditions, and the separation characteristics are improved under the guidance of the model.

In summary, our research dramatically increased the usefulness of Brownian ratchet arrays, one important class of microfabricated devices, and demonstrated two new classes of molecular separation devices: the tango arrays and the DNA prisms, which set new records in separation speed and resolution.

8.2 Future Work

The ultimate usefulness of our microfluidic devices, in the light of real world issues such as low sample concentration and purity, has yet to be established. With the use of finer lithographic tools, we expect that the devices could be scaled to separate macromolecules and supramacromolecular assemblies with great analytical precision.

Micro- and nano-fluidics have been demonstrated to be a powerful tool for the manipulation and analysis of DNA and other biological molecules. How these structures can be used to improve existing screening analysis methods, to enable new techniques, and to offer new tools for attacking fundamental questions in biology, are still great challenges for further studying.

Publications and Presentations Resulting from This Thesis

Refereed Journal Publications

- **L. R. Huang**, E. C. Cox, R. H. Austin and J. C. Sturm, "A Microfluidic Tango: Separation without Dispersion," (submitted as of Oct. 2003).
- **L. R. Huang**, E. C. Cox, R. H. Austin and J. C. Sturm, "Tilted Brownian Ratchet for DNA Analysis," ***Analytical Chemistry*** (accepted as of Oct. 2003).
- **L. R. Huang**, P. Silberzan, J. O. Tegenfeldt, E. C. Cox, J. C. Sturm, R. H. Austin and H. Craighead, "Role of Molecular Size in Ratchet Fractionation," ***Physical Review Letters*** 89**,** 178301 (2002).
- **L. R. Huang**, J. O. Tegenfeldt, J. J. Kraeft, J. C. Sturm, R. H. Austin and E. C. Cox, "A DNA Prism for High-Speed Continuous Fractionation of Large DNA Molecules," ***Nature Biotechnology*** 20(10), 1048 (2002).
- R. H. Austin, N. Darnton, **R. Huang**, J. Sturm, O. Bakajin, T. Duke, "Ratchets: The Problems with Boundary Conditions in Insulating Fluids," *Applied Physics A–Materials Science and Processing* **75**, 279 (2002).
- M. Berger, J. Castelino, **R. Huang**, M. Shah, R. H. Austin, "Design of a Microfabricated Magnetic Cell Separator," *Electrophoresis* **22**, 3883 (2001).
- N. Darnton, O. Bakajin, **R. Huang**, B. North, J. O. Tegenfeldt, E. C. Cox, J. C. Sturm, R. H. Austin, "Hydrodynamics 2-1/2 in Dimensions: Making Jets in a Plane," *Journal of Physics–Condensed Matter* **13**, 4891 (2001).

International Conference Publications

- **L. R. Huang**, J. C. Sturm, R. H. Austin and E. C. Cox, "Enhanced Brownian Ratchet Array for DNA Separation Using Flow Angle Effect," *Proceedings of the Micro-Total-Analysis-Systems 2003*, 1187 (2003).
- **L. R. Huang**, J. O. Tegenfeldt, J. C. Sturm, R. H. Austin and E. C. Cox, "A DNA Prism: Physical Principles for Optimizing a Microfabricated DNA Separation Device," *Technical Digest of the International Electron Devices Meeting* (***iedm***), 211 (2002).

- **L. R. Huang**, J. O. Tegenfeldt, J. C. Sturm, R. H. Austin and E. C. Cox, "A Microfabricated Device for Separating ~200 Kilo-Base Pair DNA Molecules in ~15 Seconds," *Proceedings of the Micro-Total-Analysis-Systems 2002*, 51 (2002).
- **L. R. Huang**, J. O. Tegenfeldt, J. J. Kraeft, J. C. Sturm, R. H. Austin and E. C. Cox, "Generation of Large-Area Tunable Uniform Electric Fields in Microfluidic Arrays for Rapid DNA Separation," *Technical Digest of the International Electron Devices Meeting* (***iedm***), 363 (2001).

International Conference Oral Presentations

- *American Physical Society March Meeting*, Austin, Texas (Mar. 2003).
- *International Electron Devices Meeting* (***iedm***), San Francisco, California (Dec. 2002).
- *Sixth International Conference on Miniaturized Chemical and Biochemical Analysis Systems*, Nara, Japan (Nov., 2002).
- *Technical Digest of the International Electron Devices Meeting* (***iedm***), Washington D.C (Dec. 2001).

Other Conference Presentations

- *Seventh International Conference on Miniaturized Chemical and Biochemical Analysis Systems*, Squaw Valley, California (Oct., 2003).